sustainability

IMPACT FACTOR 3.9

CITESCORE 5.8

Article

An HBIM Integrated Approach Using Non-Destructive Techniques (NDT) to Support Energy and Environmental Improvement of Built Heritage: The Case Study of Palazzo Maffei Borghese in Rome

Cristina Cornaro, Gianluigi Bovesecchi, Filippo Calcerano, Letizia Martinelli and Elena Gigliarelli

Special Issue
Energy Efficiency and Multi-Objective Optimization in Building

Edited by
Dr. Yi Chen and Dr. Tiezhu Sun

MDPI

https://doi.org/10.3390/su151411389

sustainability

MDPI

Article

An HBIM Integrated Approach Using Non-Destructive Techniques (NDT) to Support Energy and Environmental Improvement of Built Heritage: The Case Study of Palazzo Maffei Borghese in Rome

Cristina Cornaro [1], Gianluigi Bovesecchi [1,*], Filippo Calcerano [2], Letizia Martinelli [2] and Elena Gigliarelli [2]

[1] Department of Enterprise Engineering, University of Rome Tor Vergata, Via del Politecnico 1, 00133 Rome, RM, Italy; cornaro@uniroma2.it
[2] ISPC Institute of Heritage Science, National Research Council, Via Salaria km 29,300, 00015 Montelibretti, RM, Italy; filippo.calcerano@cnr.it (F.C.); letizia.martinelli@ispc.cnr.it (L.M.); elena.gigliarelli@cnr.it (E.G.)
* Correspondence: gianluigi.bovesecchi@uniroma2.it

Abstract: Built heritage energy and environmental improvement is increasingly being recognised as a key driver in the fight against climate change. This effort necessitates a thorough understanding of the building to guide the selection of technologies and design solutions. To have a picture of the buildings' characteristics and behaviour that is as complete as possible, in situ studies are essential, although the complexities and heterogeneities of historical buildings make these analyses still challenging, especially in professional practice. To address these issues, the paper describes an integrated approach including the field application of Non-Destructive Techniques (namely, Heat Flow Meter measurements, Infrared thermographies and indoor environmental monitoring) within a Heritage Building Information Modelling process. This interdisciplinary/integrated approach fostered the use of each type of analysis's results to guide the subsequent analyses and incrementally deepen the knowledge of the building. The methodology was applied to a case study in the historical city centre of Rome in Italy. The analyses will be of service in developing dynamic building performance simulations to support the design of the interventions.

Keywords: non-destructive techniques; heat flux meter; infrared thermography; indoor environmental monitoring; historical buildings; heritage; Heritage Building Information Modelling; HBIM; Building Performance Simulation; BPS

Citation: Cornaro, C.; Bovesecchi, G.; Calcerano, F.; Martinelli, L.; Gigliarelli, E. An HBIM Integrated Approach Using Non-Destructive Techniques (NDT) to Support Energy and Environmental Improvement of Built Heritage: The Case Study of Palazzo Maffei Borghese in Rome. *Sustainability* **2023**, *15*, 11389. https://doi.org/10.3390/su151411389

Academic Editors: Yi Chen and Tiezhu Sun

Received: 24 May 2023
Revised: 3 July 2023
Accepted: 14 July 2023
Published: 21 July 2023

1. Introduction

1.1. Energy and Environmental Improvement of Built Heritage

The number of historical buildings in Europe is estimated to be 30% of the entire existing stock [1]. Around 35% of these structures are over 50 years old, and nearly 75% of them have poor energy efficiency [2]. While the efficiency of new buildings has progressively improved over time, energy performance criteria have yet to influence the majority of Europe's existing building stock. Each year, only approximately 1% of the building stock is renovated [3]. With simple energy retrofits [4,5], buildings built before 1900 can lower their energy use by up to 60%, or by 50% to 80% with large renovations [6].

For reducing climate change, the European Union recognises the necessity of improving energy efficiency and decarbonising the current building stock. This strategy began with the Energy Performance of Buildings Directives [7,8], which established a pathway for lowering energy use in both new constructions and retrofitted existing structures. The Energy Efficiency Directives [7,9] include instruments and initiatives to modernise the construction industry and encourage building renovations. In this context, the number of European and international schemes supporting research projects, focused on the energy

efficiency of historical buildings, is rising: the Intelligent Energy Europe programme between 2007 and 2013, with SECHURBA project [10,11]; the work of the Joint Programming Initiative Cultural Heritage [12–14]; the European framework programme on research and innovation, with projects like 3ENCULT [15], RIBUILD [16], Climate for Culture [17], Effesus [18] and HeLLo [19]; the International Energy Agency task 59 "Renovating Historic Buildings towards Zero Energy" [20]. Public institutions have also developed specific guidelines to tackle interventions on energy efficiency, such as the Edinburgh World Heritage or the Italian Ministry of Culture [21,22]. The disciplinary debate, in addition to the compliance of interventions with the international restoration charters, proposed the concept of "improvement", suggesting that the energy (and environmental) response of a historical building can be improved through appropriate and well-balanced solutions, without leading to a disruption of its values, which could happen when following the wrongful assumption that the building has to be "adjusted" to current legislations and requirements [23,24].

This approach is also confirmed by the European Cultural Heritage Green Paper, a reply of the Climate Heritage Network to the European Green Deal, as the latter still fails to recognise and fully exploit the potential made available by cultural heritage in the fight against climate change [25].

Therefore, all conservation and energy improvement efforts necessitate a thorough understanding of the building to guide the selection of technologies and solutions (e.g., enhancement of energy efficiency and comfort, preservation of heritage and traditional values—including meanings, appearances and sustainable issues) [26–28]. In order to have a picture of the building characteristics that is as complete as possible, in situ studies are essential [29].

1.2. The Role of Non-Destructive Techniques

A comprehensive and informative review paper by Tejedor et al. [30] reports important information about the research trends in diagnostics, indicating a lack of investigations into quantitative techniques and emphasising the necessity to improve the research on the diagnosis of historical buildings for conservation. Indeed, very few papers have been found by the report on quantitative diagnosis, such as quantitative Infrared Thermography (IRT) and Heat Flow Meter (HFM) methods used for the evaluation of the thermal transmittance of heritage buildings. Moreover, they show how the main efforts of researchers in the last two decades have been focused on structural assessment.

Among the non-destructive techniques (NDT), IRT is a promising technology both for qualitative and quantitative diagnoses [31]. Thermographic inspections entail reading, processing, and elaborating thermal pictures that depict a temperature map of the researched object in false colour. The qualitative technique IRT entails determining the object's hotter and colder points in relation to the surrounding environment, and then correlating the anomaly with the discovered temperature differential [32]. As a result, this method aids at establishing the thermal pattern and ascertaining where (and how extensive) thermal anomalies are (i.e., the location of thermal irregularities). Because of its widespread use and its non-invasive characteristic, IRT has benefited building diagnosis in general [33–35]. Concerning historical buildings, most of the papers are focused on walls and are mainly devoted to crack detection [36–40], health and structural state [41,42], as well as moisture, humidity, and rising dampness assessment [43–47]. When combined with other NDT techniques, IRT can provide a thorough understanding of architectural features, construction techniques, infills or previous openings, as well as back hypotheses on building phase constructions, due to the ability to detect different materials beneath the plaster coating [48,49].

One of the primary goals of quantitative diagnosis, to support energy and environmental improvement interventions, is to evaluate a building's thermal characteristics. However, little research has been done on historical structures. The thermal transmittance (commonly named the U-value) quantifies the amount of heat that travels through the building envelope when a sufficient temperature differential (10–15 °C) exists between the two sides [50,51],

and it is the fundamental determinant of thermal characteristics. It can be evaluated using the following NDT methods: the theoretical method (regulated by ISO 6946:2007 [52]); the HFM method (regulated by ISO 9869-1:2014 [53]); the thermometric method [54] (based on ISO 9869-1:2014 [53]); quantitative IR thermography [55–57], and the simple hot box method [58,59].

The theoretical method calculates the U-value based on the thickness of each layer of the building envelope (retrieved from documentation and building projects, or by analogy with contemporary buildings) and the corresponding thermal conductivity; technical standards, material datasheets and databases can help [52]. This approach can be employed for homogeneous or multi-layered construction elements in steady-state settings. However, because historical elements are often inhomogeneous (i.e., with different materials, cavities with air flows, joints, varied thicknesses, etc.) [60,61] and there is a lack of databases on pre-industrial materials and technologies (with very few examples [60,61]), the analytical computation of their thermal performances appears critical. Quantitative IR thermography is attracting more attention recently [62,63] because it is a relatively fast procedure compared to the more classical HFM method. Both methods allow for measuring the U value of a wall directly in situ. Focusing the attention on HFM, it must be noticed that only a few works in the literature strictly regard the application of this technique to historical buildings [61,64–68]. An interesting approach involves using HFM measurements and numerical models to evaluate the thermal characteristics of both standard and historical buildings through inverse methods. These methods can be applied using an exhaustive search strategy or an optimisation process. In this instance, the goal is to reduce the difference between computed values based on the estimated attributes (thermal characteristics) and measured values (such as temperature or heat flux) [69–73].

Finally, researchers have focused their attention on specific aspects of the study of historical buildings, such as wall stratigraphy, the conservation of wooden floors or the supporting walls of paintings and mosaics [74–81].

The considered literature stresses how the study of heritage buildings necessitates a wide range of processes and experiences, because a multidisciplinary approach is the most effective way to gain a thorough understanding of the structure from various perspectives (historical, architectural, seismic, energetic, etc.) [64,82,83]. In situ analyses should be coupled with other types of investigations, such as historical and architectural analysis, geometric surveys and conservation state analysis, which help to identify construction techniques, materials and stratigraphies, and characterise the evolutions and modifications of the building [23,84,85]. This is paramount for assessing heterogeneous structures with high levels of uncertainties, where analytical and non-analytical procedures should be combined to achieve the best possible rational formulation of a problem on the basis of data, hypothesis and interpretation [86]. Moreover, the data collected, in addition to coming from extremely diverse sources, are also subject to continuous changes, reinterpretations, inconsistencies and gaps that must be identifiable until the end of the process and beyond.

Therefore, an integrated approach is crucial for the energy and environmental improvement of historical buildings, including their preservation and enhancement, and there is an urgent need for interoperability among different NDT techniques [30].

1.3. The Role of Heritage Building Information Modelling

To this end, a well-established methodology for the management and representation of knowledge is Building Information Modelling (BIM), defined as the creation of a shared digital representation of a built asset that centralises all the data pertaining to it [87,88].

BIM is based on the integration of both geometric and semantic information, associating the 3D representation of building elements through model objects to alphanumeric data and documents; the relationships among said objects are expressed as the "behaviour" of the building [89]. The application of this information system to built heritage is commonly referred to as Heritage BIM (HBIM), acting as a single repository for documentation, diagnostics, monitoring, energy and environmental data, and analytical investigations and

surveys, enhancing the dynamic implementation of evolving knowledge through time and reducing the risk of data obsolescence and loss [90–92]. This approach also strengthens the interactions among different experts in the built heritage sector, thanks to its multiple tools for data modelling, visualisation and representation [93].

Each BIM process and the subsequent models use shape data acquisition procedures and modelling strategies [94,95]. The possibility of collecting and representing, in an HBIM model, data from NDT analyses could improve the current knowledge of the building conditions and behaviour, and help design and compare improvement scenarios. However, this is a difficult task, given that the most widespread BIM authoring applications do not have specific tools, nor are there shared procedures among the experts in the field, to represent this type of information, which can be heterogeneous in nature and or/include multiple values (e.g., comprised of visual thematic maps, heat plots, tables), or not be directly associated to a BIM object (e.g., referenced to a single part of an object or encompassing more objects, such as a decay map for an entire façade) [84,96]. On the contrary, information is generally embedded into BIM objects via sets of properties, whose values have unique data types, are unique for each object and cannot be nested; moreover, abstract information, not referring to specific objects, is challenging to integrate [89,97]. Examples of field analysis representation within an HBIM model focus especially on conservation state assessment, damage evolution monitoring and stratigraphy depictions [98–106].

To enhance data integration and data sharing, the BIM approach encompasses the concept of Common Data Environment (CDE), defined as the agreed source of information for any given project or asset, generally in the form of a web-based file repository, for collecting, managing and disseminating information among the actors involved [87]. In a CDE, therefore, different data sources can be hierarchically organised and shared; however, especially when files and formats are not directly interoperable, data management requires strict operating procedures and protocols to ensure information consistency, durability and quality [107,108]. A well-structured CDE could support the direct and indirect integration of data and results from NTD analyses in BIM models through linked reports, documents, images, databases and tables. Within an energy and environmental improvement process, this organised set of models and information containers in a CDE could be used as input data to be mapped and exported to a Building Performance Simulation (BPS) application, to simulate the current and future energy efficiency and thermal comfort of the building [109–111]. Tests on BIM-supported dynamic BPS are also starting to grow in application to historical buildings, despite the additional complexities involved in the task [85,86,112–116].

1.4. Research Aim

This study aims to present a methodology and field application of NDT analyses (namely, HFM, IRT and indoor microclimate monitoring) to support BPS calibration and the simulation of energy and environmental improvement interventions of a historical building within an HBIM process. It was implemented in Palazzo Maffei-Borghese, the Italian case study of ENI CBC Med BEEP Project (BIM for Energy Efficiency in the Public Sector) [85]. The main objective of the BEEP project is to propose a methodology for the development and financing of the energy and environmental improvement of historical public buildings in the Mediterranean through the use of BIM and BPS, as advanced tools to better develop design solutions and support Energy Performance Contracting activities [117].

The project's objectives frame the methodology applied to this study as a technological transfer to professional practice, thus also considering time, cost and available skill constraints. This guided the research towards a trade-off between the degree of knowledge obtainable on the building and these constraints [86,118].

1.5. Research Gap and Noverlty

Historical buildings limit the type of analysis that can be performed (which must be non-destructive and non-invasive) in yielding a clear picture of their energy and environ-

mental characteristics and behaviour. Moreover, given the heterogeneity and complexity of built heritage, the implementation of available diagnostic technologies often requires ad-hoc solutions. Within this framework, the literature review highlights a few research gaps:

1. lack of consolidated data on the characterisation of historical buildings;
2. lack of a consolidated interdisciplinary process of data collection on historical buildings;
3. lack of field application studies on the topic describing in detail the limitations, challenges and solutions proposed;
4. need to tailor existing analysis and design methodologies and tools to historical buildings' specificities and complexities.

To address these gaps, the novelty of this study relies on the integrated approach proposed to diagnostics, capable of merging the insights of several pipelines, such as historical and architectural analysis and geometric surveys, with NDT in situ measurements in a single interdisciplinary HBIM workflow, to optimise the measuring process, strengthen the results' reliability and reduce time and costs. Moreover, the study tackles the highlighted lack of applications and data of quantitative NDT to historical buildings for energy and environmental improvement [30]. Furthermore, the combination of HFM measurements, conventional standards and dynamic simulations to determine the thermal transmittance of wall packages represents a significant novelty, and helps to improve the accuracy of the results.

2. Case Study Description

Figure 1 shows the position of the case study: the building of Palazzo Maffei-Borghese is located in the historic centre of Rome, in the district called Campo Marzio. The four-storey office building, with a net surface of about 3500 square meters, is one of the headquarters of the Legal Council of the State (Avvocatura Generale di Stato), owned by the State Property Agency (Agenzia del Demanio), and it is recognised as having historical, artistic and archaeological significance by the Ministry of Culture. Apart from the entrance, lobby area and two stairways, the ground floor of the building is occupied by the Judicial Records Office; this section, while important to an understanding of the building as a whole, is a restricted area and therefore was excluded from subsequent analyses and simulations. The building is located a block south of Palazzo Firenze, and its origin dates back to a small late medieval domus. Antonio Tempesta's plan of 1593 shows a one-story building surrounded by a courtyard, which was originally an urban hortus (garden). This type of mixed architecture made of built and green spaces was common in the suburban areas of Rome in the transition period between the 15th and 16th centuries. The current state of the building is the result of a substantial late 19th century intervention that integrated the irregular huts in a homogeneous palace, according to the forms of Umbertinian neo-Renaissance academism, with Renaissance revival influences [119,120].

Figure 1. Position of the case study.

Figure 2 shows the façade that overlooks via del Clementino, formerly Via Trinitatis, near the junction with Via di Ripetta. In 2004, the building went through a restoration that involved a structural consolidation, which rebuilt part of the slabs and roofs, consolidated walls and changed the internal room distribution, adding new toilets and a new internal stairwell. The HVAC (Heating Ventilation Air Conditioning) layout was renovated by installing a coupled gas boiler and heat pump generator system with fan coils as main terminals, although keeping radiators in some spaces; a mechanical ventilation system was added, but never put into operation.

Figure 2. Palazzo Maffei-Borghese, Rome, Italy.

The case study was tackled by an interdisciplinary team including experts in conservation, environmental design, energy and environmental analyses, HBIM, BPS and interoperability.

3. Methods

3.1. Description of the General Approach and the Specific Analyses Workflow

Figure 3 shows the methodology workflow applied to the case study.

As shown in the left heading in Figure 3, the entire process was divided into two main phases. Phase 1 consisted of developing a solid understanding of the building characteristics through a series of analyses: a historical and architectural analysis, a geometric survey with both traditional and innovative techniques, a general conservation state analysis (materials and structure survey) and a robust environmental and energy analyses, which comprised several interdisciplinary activities through the application of NDT techniques. These diagnostics pipelines, advanced over different periods, were integrated within an HBIM model in a CDE, which was developed and revised iteratively by the interdisciplinary team each time new data were gathered. The first model is based on historical

and architectural analysis, a geometric survey and technical documentation, providing data mainly on building morphology, construction systems and HVAC. The following updates of the model progressively integrated the results of IRT, HFM and the other in situ field measurements to refine the characterisation of stratigraphies and user profiles. Phase 1 ended with the interoperability between HBIM and the simulation model, which was validated through a calibration process using energy bills and monitoring data. Phase 2 regarded the design of interventions and the simulation and evaluation of the best solutions. The end of phase 1 and all of phase 2 are out of the scope of the current paper; more information can be found in [85].

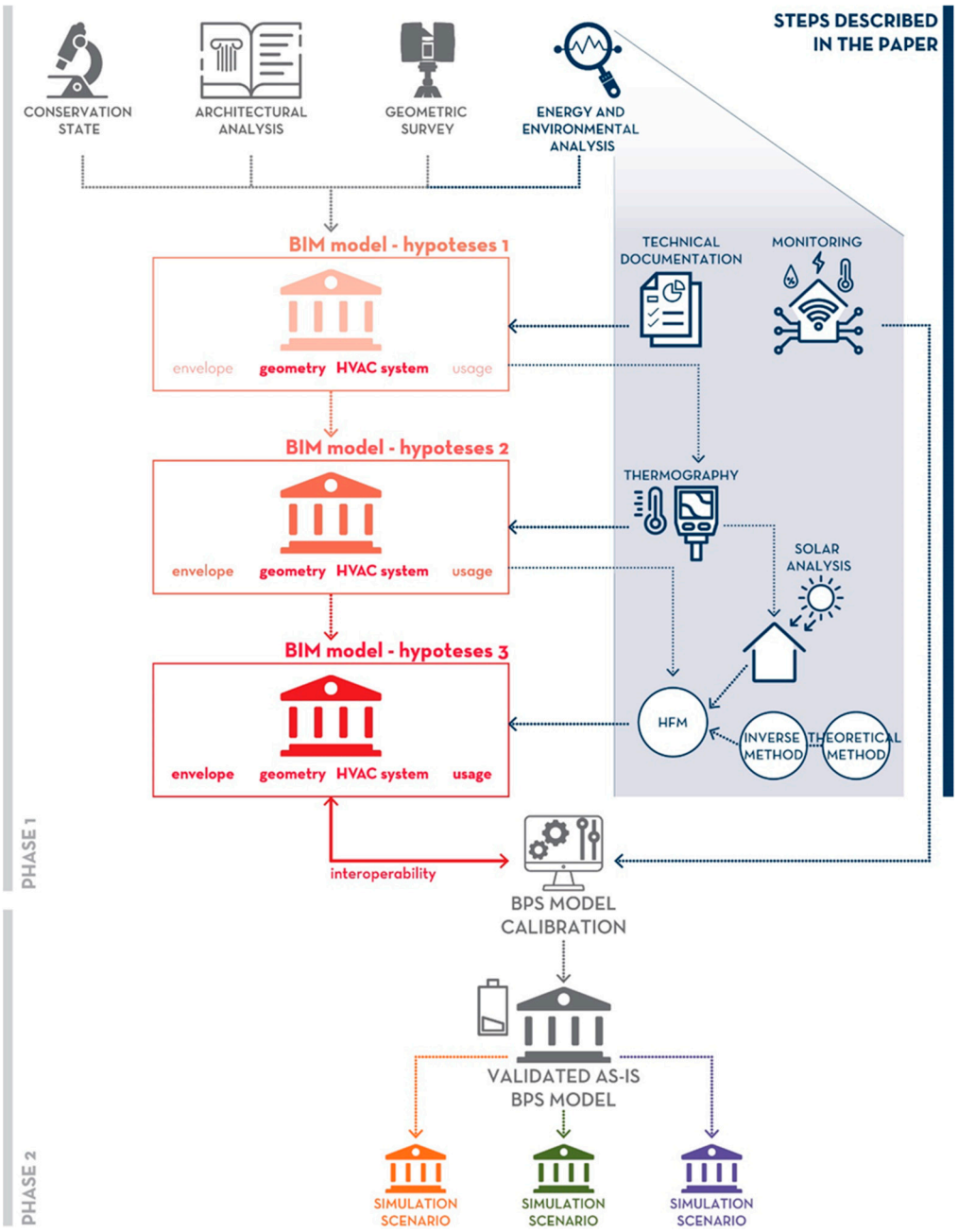

Figure 3. Graphic representation of the methodology workflow. The blue colour highlights the steps of the methodology that pertain to the current paper.

Focusing on the energy and environmental NDT analyses, to obtain a thermophysical characterisation of the building envelope and to corroborate the results of other analyses re-

lated to construction techniques, stratigraphies, building use and passive/active behaviour, three field analyses were carried out.

These are the core of this study: an IRT campaign for the entire building, nine HFM measurement points (seven on the walls and two on the roofs) and a year-round monitoring of the indoor climate in eight key spaces of the building.

All the data were gathered according to a specific protocol to ensure the required data mapping for the BIM to BPS interoperability. Each new analysis was integrated into the HBIM model directly or via the CDE, thanks to the flexibility and ease of modification of the HBIM model through time. This contributed to the incremental knowledge of the building and to more and more refined hypotheses on its geometry, the thermophysical characterisation of the envelope, the HVAC systems and the usage profiles. Such detailed knowledge was then used to calibrate a dynamic simulation model of the building's current state [85].

The historical–architectural analysis and the geometric survey allowed the team to develop a first hypothesis on the main building parts composing Palazzo Maffei-Borghese, the constructive system of the building and the characterisation of its envelope. The hypothesis was drafted from a study of restoration manuals of Rome, the area of Campo Marzio (where the building is located) and contemporary buildings, such as Palazzo Firenze (which is part of the same block), integrated with the investigation of wall thicknesses, internal height changes and façade alignments, the presence of vaults and the spatial organisation of the building. For the elevation structures, the study suggested the presence of either load-bearing rubber masonry with a tuff wall layer or simple tuff load-bearing masonry for the walls, and of steel beams with segmented hollow or solid brick vaults for the slabs [121,122].

As for the main building parts, the geometric survey highlighted a reduction in the wall section from the ground to the upper floors, and a height difference in the internal floors (marked by five steps) in correspondence with the joints between a main block, revolving around an internal cloister identified as Part-01, and the rest of the building. Part-01 is also recognizable thanks to the different alignments and the richness of the decorations of the façade (Part-01 and Part-02). Cross-vaulted rooms with decorated balconies on a portion of the building facing the inner courtyard suggested the presence of another different block (Part-03), as well as the configuration of the joints between Part-01 and 03 (Part-04). Part 05 is a roof substitution and addition, datable to the last restoration of 2004, and it is characterised by a concrete structure with hollow brick masonry and hollow bricks and concrete slabs.

This hypothesis sets out a layout of five parts, possibly marked by different construction systems, and has helped us develop specific questions to be examined/checked with specific NTD analyses: first with IRT, then deepened with HFM and the indoor microclimate monitoring of temperature and relative humidity. To support the management of these NDT analyses, the building façade was further subdivided into nine vertical sectors, depending on orientation and morphology, and five horizontal ones (four floors and the roof).

Figure 4 shows this discretisation in plan and façade, representing, with the same colour, the five homogeneous parts (with the same construction systems) hypothesised by the preliminary results of the analyses. The restricted section of the building, not belonging to the "Avvocatura Generale dello Stato", is represented with a diagonal hatch.

The IRT aimed at identifying discontinuities among the envelope of the building, focusing on checking the variations between the ground floor and upper floors (to verify any residuals prior to the 19th century phase) and the junctions between the initially hypothesised five parts. The survey identified 11 heterogeneous stratigraphies, i.e., envelope elements differing either by material, construction system or thickness, consistent with a possible reduction in the homogeneous parts to three (Part-01, Part-02-03-04 and Part-05, see Results). Figure 5 shows this updated subdivision.

Figure 6 shows a matrix depicting the subdivision of the façade, with the columns representing the building sectors and the rows representing the floors and roof of the building. The table summarises the consolidated hypothesis of homogeneous envelope

types according to the IRT field study. Portions (cells) belonging to the same part have the same colour shade; a difference in the lightness of colour indicates a different thickness, attributable to a narrowing of the wall section of the same construction system. The pattern of diagonal lines denotes a construction typology derived from similar wall elements. Each stratigraphy within the parts (identified at this stage of the analysis) is represented by a letter.

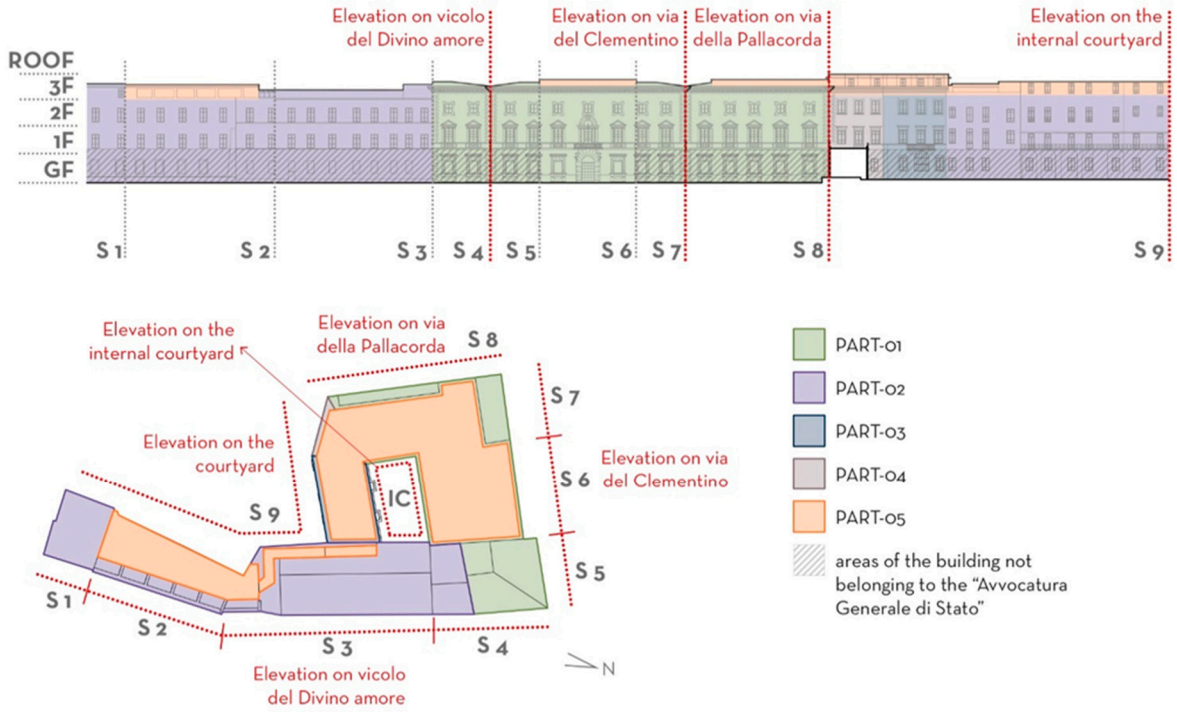

Figure 4. Plan and façade of the building, representing the first subdivision into parts and sections (S) resulting from preliminary analyses.

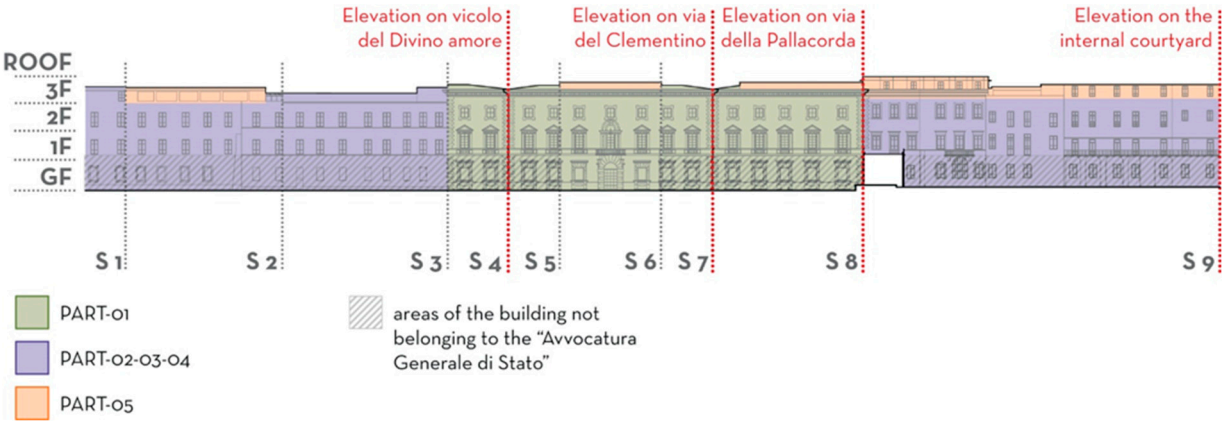

Figure 5. Updated hypothesis of subdivision of the building into 3 parts and 9 sections (S).

Subsequently, thanks to the support of preliminary historical and architectural analyses and geometric surveys, the team agreed that measuring 9 homogeneous envelope stratigraphies (2 of which are on the roofs) with HFM, out of the 11 identified, was enough to characterise the whole building's opaque envelope, considering also time/cost constraints. One discarded stratigraphy (E) belongs almost entirely to the Judicial Records Office, the other public body hosted on the premises, and historical and geometrical evidence supports its belonging to Part-01 and having the same construction system and materials of stratigraphies F and G, but with different thicknesses. The same applies to the other discarded

stratigraphy (I), which is a small surface of a flat roof, with the same construction system and materials, and different thickness from J in the newly constructed Part-05.

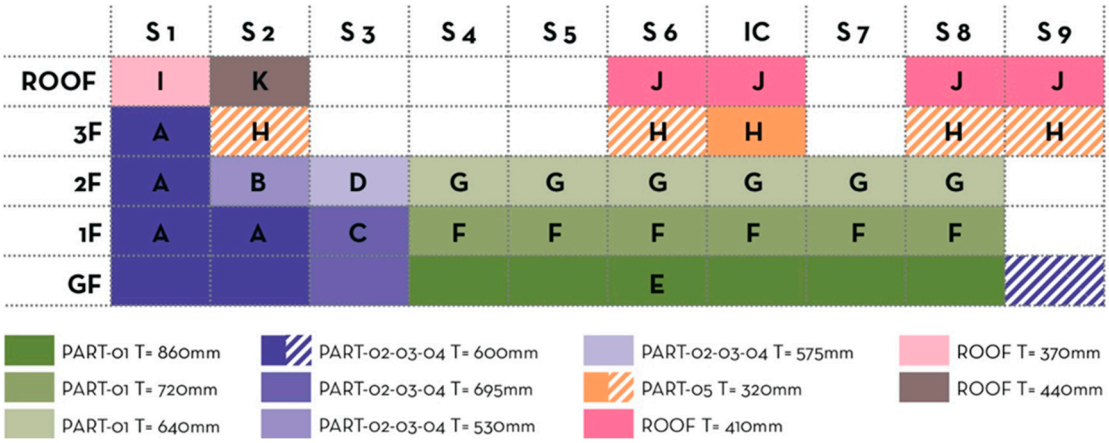

Figure 6. Matrix of the building façades' subdivision.

Given the extension of homogeneous surfaces (stratigraphies) to be analysed and the limited time available, it was decided to optimise the location of the measurement points by performing a sunshine duration simulation on the building facades, to select the points with the least solar irradiance contribution on the walls. To this end, a simplified 3D model of the building was created including the shapes of the openings, so as to better pinpoint the results on the facades. Figure 7 shows the graphical output of the sunshine duration analysis: a southwest view of the main courtyard, showing the number of direct sunlight hours on the façades of the building in a blue-to-red scale. The surrounding buildings were modelled as simple volumes; the trees (in green) are composed of two cross-oriented two-dimensional shapes, so as to not excessively overburden the calculation, while maintaining a satisfactory representation of their shading effect. The simulation was carried out in the months available for the HFM survey using the Ciampino Airport meteorological and climatic file. The software combination of Rhinoceros Rhino 7, with its Visual Programming Language and environment Grasshopper and the environmental analysis plug-in Ladybug, was used for the simulation. The analysis grid on the building (the tessellation of the surfaces in calculation units) was set to 1 m^2.

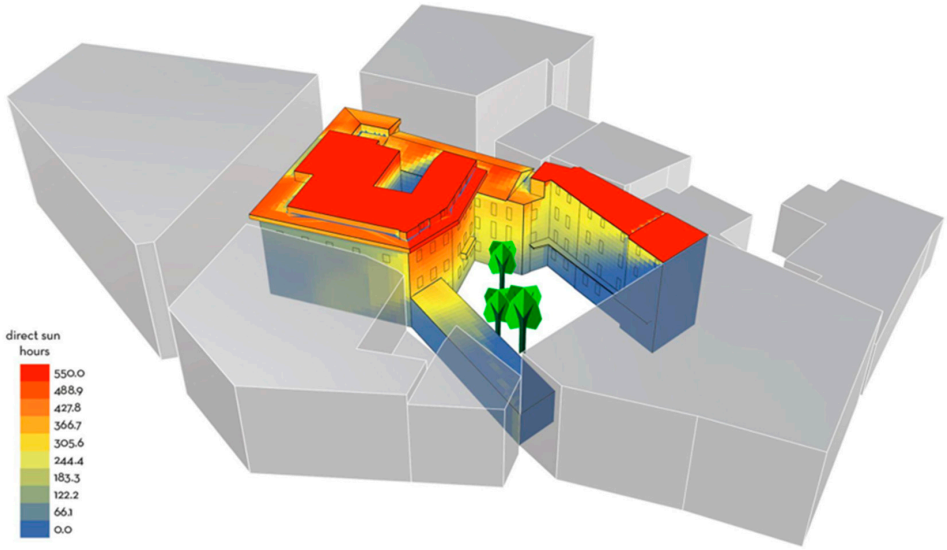

Figure 7. Graphical output of the sunshine duration analysis.

The graphical output of the simulation allowed the selection of the best portion to perform the HFM measurements for each of the nine homogeneous stratigraphies—generally a portion of the façade with two to five rooms under direct sunshine for the shortest time.

Figure 8 shows the matrix with the sunshine hours on the building façades for January and February; the blue-grey areas indicate low irradiation. The letters define homogeneous envelope stratigraphies (see Figure 6), while the white letters indicate the areas selected for HFM analysis.

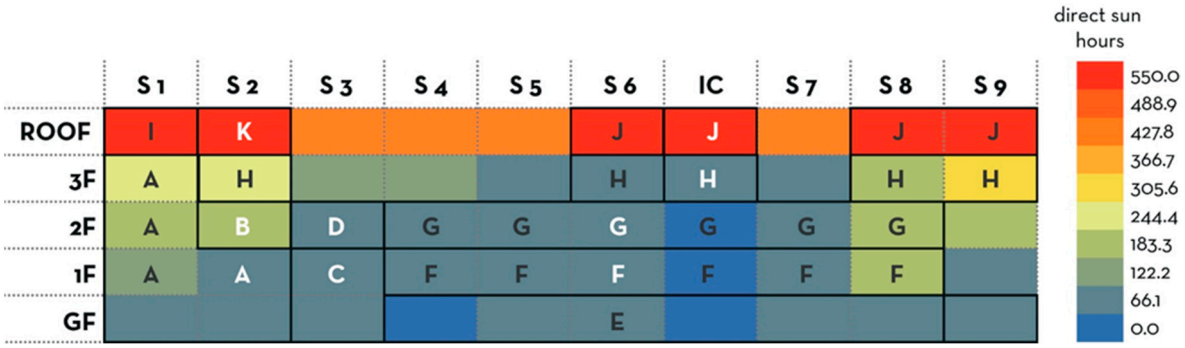

Figure 8. Sunshine hours matrix on the building façades.

While the pipeline of IRT and then HFM proceeded from November 2020 to March 2021, the indoor microclimate monitoring of temperature and relative humidity of key rooms of the building started at the end of December 2020. The eight rooms to be measured were selected, aiming at:

- studying rooms with the most common construction systems that emerged in the integrated analysis;
- analysing at least one room used continuously and one occasionally (to have a description of the most common types of uses, with also a different density of occupants in the room);
- monitoring the intermediate floors and understanding the behaviour of the building in portions that are less influenced by external forcings;
- covering as many exposures as possible;
- monitoring the office reception on the ground floor, as it is a very thermally dispersive space with discomfort issues, and the full-height internal gallery of Part-01 (Figure 4);
- studying the synergies between two "connected" rooms, one above the other.

3.2. IR Thermography Method

Thermography is a non-destructive diagnostic technique that measures the infrared radiation emitted from an object and can determine its surface temperature.

A body that has a certain temperature emits electromagnetic radiation in the infrared range (IR), which is generated by the oscillatory and rotational movements of the molecules and atoms that make up the substance.

A body at room temperature emits infrared radiation with a wavelength of about 10 µm.

By measuring the radiation emitted by a body, it is possible to determine its temperature using the Stefan–Boltzmann law [123],

$$\dot{Q} = \varepsilon \cdot \sigma \cdot A \cdot T^4 \quad (1)$$

where $\dot{Q}$ is the thermal radiation power in Watt, ε is the body emissivity ($0 < \varepsilon < 1$), σ is the Stefan–Boltzmann constant ($\sigma = 5.67 \cdot 10^{-8}$ W $\cdot$ m^{-2} $\cdot$ K^{-4}), A is the surface in m^2 and T is the temperature in Kelvin.

A real surface can not only emit thermal radiation, but also absorb, reflect or transmit the thermal radiation incident on it. In particular, opaque surfaces (such as the walls of a building) can only absorb and reflect this radiation. So, an opaque surface not only emits radiation due to its temperature, but also reflects a certain amount of radiation emanating from the surrounding bodies. The thermal radiation (emitted and reflected) that leaves the surface as a whole is called radiosity. When a surface is observed with the thermal imager, it measures its radiosity, i.e., the contribution of the radiation reflected from the surface itself. Therefore, the temperature T of the examined surface is disturbed by the other bodies surrounding it, which have a certain temperature, the so-called reflected temperature.

The direct reflector method is a simple method of measuring reflected temperature (background temperature) that can introduce an error into thermography. The method consists of using a crumpled aluminium sheet that has the task of reflecting the radiation incident on the surface (reflector). The aluminium sheet is placed on the area to be examined and its temperature is measured with the thermal imaging camera. Since it is a highly reflective material, the camera does not record its temperature, but the thermal radiation it reflects (T_r). Knowing T_r, the effect of the background temperature can be compensated [124].

Another important disturbance factor in these cases is the operator itself, who is seen in the room via their heat radiation and disturbs the measurement. To avoid this, it is usually sufficient to vary the shooting angle and notice the differences. In any case, the recording angle must be within a range of $\pm 45^{\circ}$ with respect to the façade standards, in order to avoid or limit the reflected radiation from the operator.

The thermal imager is thus capable of producing images in greyscale or false colours that represent the thermal state of the areas being examined. In this process, each temperature value is assigned a corresponding colour, with a sensitivity that can even reach a few hundredths of a degree.

The thermographic survey of the building is primarily used to identify discontinuities among envelope sections and to verify the hypotheses of the preliminary results from the historical and architectural analyses and the geometric survey. The new hypotheses are used to define the number and location of the HFM measurement points, so as to acquire a solid understanding of the building envelope.

Five inspections were carried out in the period between December 2020 and February 2021.

3.3. HFM Method

The procedure for measuring the transmittance U consists in measuring the heat flux through the wall and the indoor and outdoor air temperatures, T_i and T_e, or the corresponding surface temperatures $T_{w\text{-}i}$ and $T_{w\text{-}e}$ (if we want to measure the conductance C) over sufficiently long periods.

The HFM consists of a thin layer of a material with known and stable thermal resistance. The temperature difference across this layer is measured with a set of thermocouples connected in series (thermopiles). The system is housed in a moisture-proof protective case with good mechanical properties. By measuring the temperature on both sides of the plate (which depends on the current flowing through it) using a suitable calibration curve, the measurement of the heat flux is obtained directly. It is important that the plate is suitably thermally coupled to the element under investigation to minimise contact resistance, and that it is connected to a data logger.

The data from the measurements with the HFM can be processed according to the standard ISO 9869-1:2014 [53] using the progressive average method.

The progressive average method consists in calculating the conductance C or the heat transfer coefficient U by using, at each time point, the average values of all previous time points. For masonry with a high thermal mass, the measurement cycle must be at least 72 h, taking into account multiples of a complete cycle of 24 h.

An estimate of the conductance and the heat transfer coefficient can be made using the following equation [123]:

$$C = \frac{\sum_{j=1}^{n} \dot{q}_j}{\sum_{j=1}^{n} \left(t_{wi-j} - t_{we-j}\right)} \qquad \left(\mathrm{W \cdot m^{-2} \cdot K^{-1}}\right) \tag{2}$$

where $\dot{q}$ is the heat flux per unit area in $\mathrm{W \cdot m^{-2}}$, t_{wi} and t_{we} are the temperatures of the wall's inside and outside in degrees Celsius, and C is the conductance of the wall in $\mathrm{W \cdot m^{-2} \cdot K^{-1}}$.

$$U = \frac{\sum_{j=1}^{n} \dot{q}_j}{\sum_{j=1}^{n} \left(t_{i-j} - t_{e-j}\right)} \qquad \left(\mathrm{W \cdot m^{-2} \cdot K^{-1}}\right) \tag{3}$$

where $\dot{q}$ is the heat flux per unit area in $\mathrm{W \cdot m^{-2}}$, t_i and t_e are the ambient internal and external temperature in degrees Celsius and U is the overall heat transfer coefficient in $\mathrm{W \cdot m^{-2} \cdot K^{-1}}$.

The final value should be the one closest to the actual value of the structure under investigation. Usually, this asymptotic value is close to the real value when the thermal transmittance obtained differs no more than 5% from the value obtained 24 h before.

An inverse method was also used to double-check and validate the measured results, and for the parametric identification of the thermophysical properties of the unknown materials of the layers of the investigated walls (namely, the equivalent thermal conductivity λ and the equivalent heat capacity $\rho \cdot c_p$). This was done by comparing and minimising the difference between the results coming from the HFM data and those resulting from a numerical model of the masonry. Figure 9 shows a conceptual scheme of the masonry package model and a synthesis of the optimization process.

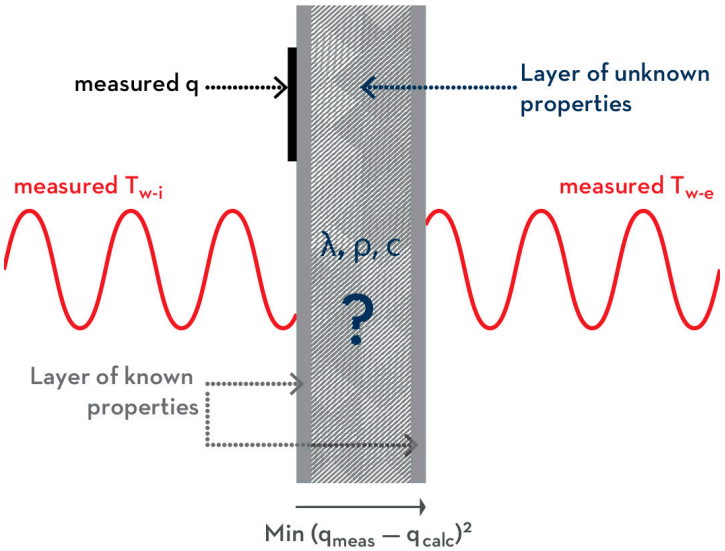

Figure 9. Conceptual scheme of the masonry package model.

For each unit of measured masonry, a wall package model was created in the dynamic simulation software for buildings, IDA ICE 4.8 (EQUA Simulation, Stockholm, Sweden).

For each package, different layers were assumed, based on the study of the building's historical construction techniques and the literature on the thermophysical properties

of wall masonries [125,126] including the standards UNI/TR 11552:2014 [127] and UNI 10351:2021 [128].

A genetic optimisation algorithm (Genopt), integrated into the software IDA ICE, was used to identify the equivalent thermophysical properties (thermal conductivity, density and specific heat) of the unknown materials by minimising the difference between the heat flux measured during the campaign and that calculated by the simulation.

The trends of the measured temperatures of the internal and external surfaces of the masonry were set as boundary conditions of the model.

The equivalent thermophysical properties of the layer so determined were used to calculate the equivalent conductance of the package.

4. Experimental Set-Up

4.1. Measurement Equipment

The thermal imagers used for the thermography campaign is a Fluke model Ti32 9 Hz (Fluke, Everett, WA, USA); Table 1 reports the main specifications of the model used.

Table 1. Specifications of the thermal imager (Fluke Ti32-9Hz).

Main Specifications	
Detector type	Focal plane array uncooled microbolometer
Resolution	320 × 240 pixels
Noise Equivalent Temperature Difference (NETD)	≤0.045 °C (45 mK)
Infrared spectral band	7.5–14 µm (long wave)
Minimum focus distance	46 cm
Temperature measurements range	−20 °C to 600 °C
Temperature measurements accuracy	±2 °C or 2%
Image capture frequency	9 Hz
Lens Type	
Field of view	23° × 17°
Spatial resolution (IFOV)	1.25 mRad
Minimum focus distance	15 cm

The experimental apparatus for the thermal transmittance measurements consist of a heat flux meter to measure the heat flow (Almeno FQA017, Ahlborn, Holzkirchen, Germany), two temperature sensors to measure the temperature of the walls or the inside and outside air (Almeno FTA390), and a data acquisition system (Almeno 2590-4AS); see Table 2 for the specifications.

Table 2. Main specifications of the sensor used in HFM.

	Producer	**Model**	**Type**	**Temp. Range**	**Accuracy**
HFM	Ahlborn	Almeno FQA017C	117	−40–80 °C	5% @ 25 °C
Thermocouples	Ahlborn	Almeno FTA3901L03	NiCr-Ni	−25–400 °C	Class 2 (DIN/IEC 582/2)

The indoor temperature and relative humidity measurements were carried out using the Bluetooth Smart Gadget Datalogger SHT31 (Sensirion AG, Staefa ZH, Switzerland), shown in Figure 10, a battery-powered data acquisition system that is capable of measuring

relative humidity and air temperature, is compact and lightweight, and is intended for indoor use (see Table 3 for the specifications).

Figure 10. Smart Gadget Datalogger.

Table 3. Datalogger specifics.

	Relative Humidity	Temperature
Accuracy	±2%	±0.3 °C
Resolution	0.01%	0.015 °C
Measurement range	0–100%	−40–125 °C
Response time	8 s	>2 s

The data logger can be configured via Bluetooth with a tablet or smartphone and the "Sensirion MyAmbience 3.1.0" app.

4.2. Sensor Positioning

Tables 4 and 5 show the list of sensors installed in the rooms and the information needed to identify their position in the building, as shown in Figure 11. The tables and the figure depict the locations of the sensors for the measurement of thermal transmittance (HFM) and for microclimate monitoring (Microclimate). The sensors were located in the key environments of the building to provide representative information on the different uses of the rooms (Microclimate) and on the construction characteristics and orientation of the building (HFM), as already explained in Section 3.1. HFM sensors were located in a representative portion of the surface of the wall under investigation to avoid edge effects and direct solar radiation. The locations selected for the HFM measurements are the result of the information obtained from the historical investigation of the building, the thermographic measurements and the simulation of the sunshine duration. As regards the positioning of indoor microclimate sensors, rooms 209, 220 and 247 provide information on the behaviour of rooms facing opposing exposures (respectively, northeast and southwest), rooms 322 and 344 on high-density occupancy, room 138 on typical low-density occupancy, and room 208 on an internal service space (full-height internal gallery). Room 003 (office reception) was chosen due to its high thermal dispersion and discomfort issues, as it is highly influenced by the outdoor climate, being a walk-through space.

Table 4. HFM sensors list and placement.

Activity	Sensor #	Room Code	Floor	Exposure	Type of Masonry (Figure 6)
HFM	1	220	2	Northeast	D
HFM	2	116	1	Northeast	C
HFM	3	127	1	East	A
HFM	4	234	2	East	B
HFM	5	105	1	Northwest	F
HFM	6	209	2	Northwest	G
HFM	7	318	3	South, Internal Cloister	H
HFM	8	318	3	Roof	I
HFM	9	344	3	Roof	K

Table 5. Environmental monitoring sensors list and placement.

Activity	Sensor #	Room Code	Floor	Exposure, Use, and Density of Occupancy
Microclimate	1	003	G	Not applicable, office reception, low density of occupancy
Microclimate	2	138	1	Southeast, office, low density of occupancy
Microclimate	3	208	2	Not applicable, full-height internal gallery, service space
Microclimate	4	209	2	Northwest, office, low density of occupancy
Microclimate	5	220	2	Northeast, office, low density of occupancy
Microclimate	6	247	2	Southwest, office, high density of occupancy
Microclimate	7	322	3	Southwest, office, low density of occupancy
Microclimate	8	344	3	West, office, high density of occupancy

Figure 11. Locations and sensors code for indoor microclimate monitoring and HFM analysis divided by floor.

The rooms have not been taken out of service. Possible interference from the passage of people was taken into account by positioning the sensors further away from the workplaces, so that we could exclude the presence of users during the measurements.

Figure 11 depicts the position of the sensors for HFM and monitoring in the different floors of the building. Figure 12 shows a picture of the sensor installation for HFM measurement in six of the nine rooms under investigation.

Figure 12. Example of installation of sensors for HFM measurements in 6 of the 9 rooms.

5. Results and Discussion

5.1. IR Thermography

The thermographic campaign was carried out from December 2020 to February 2021 with five surveys with approximately 600 shootings, undertaken early in the morning to avoid the influence of solar radiation.

Concerning the exterior of the building, the surveys made it possible to evaluate:

1. thermal bridges' form and structure;
2. different construction materials;
3. discontinuities.

Relative to the inside of the building, the qualitative survey allowed the team to identify window installation errors resulting in air infiltrations, as shown in Figure 13.

The methodology used for determining the thermography of the external envelope was aimed at identifying discontinuities in behaviour between portions of masonry.

During the measurements, several problems arose in carrying them out correctly. The first difficulty was strictly related to the context of the analysis, i.e., the historic centre of Rome, where the narrow streets do not allow for correct shooting distances and angles. This problem was minimally reduced by using different optics, including a lens with a smaller focal length and a larger shooting angle.

It was indeed difficult to shoot a large part of the façade, to compare the different buildings under the same shooting conditions. In the vertical plane, this becomes even more challenging due to the need to shoot from below and to have a larger shooting angle, which results in a larger angle of incidence, causing the temperature of the sky to be reabsorbed by reflection.

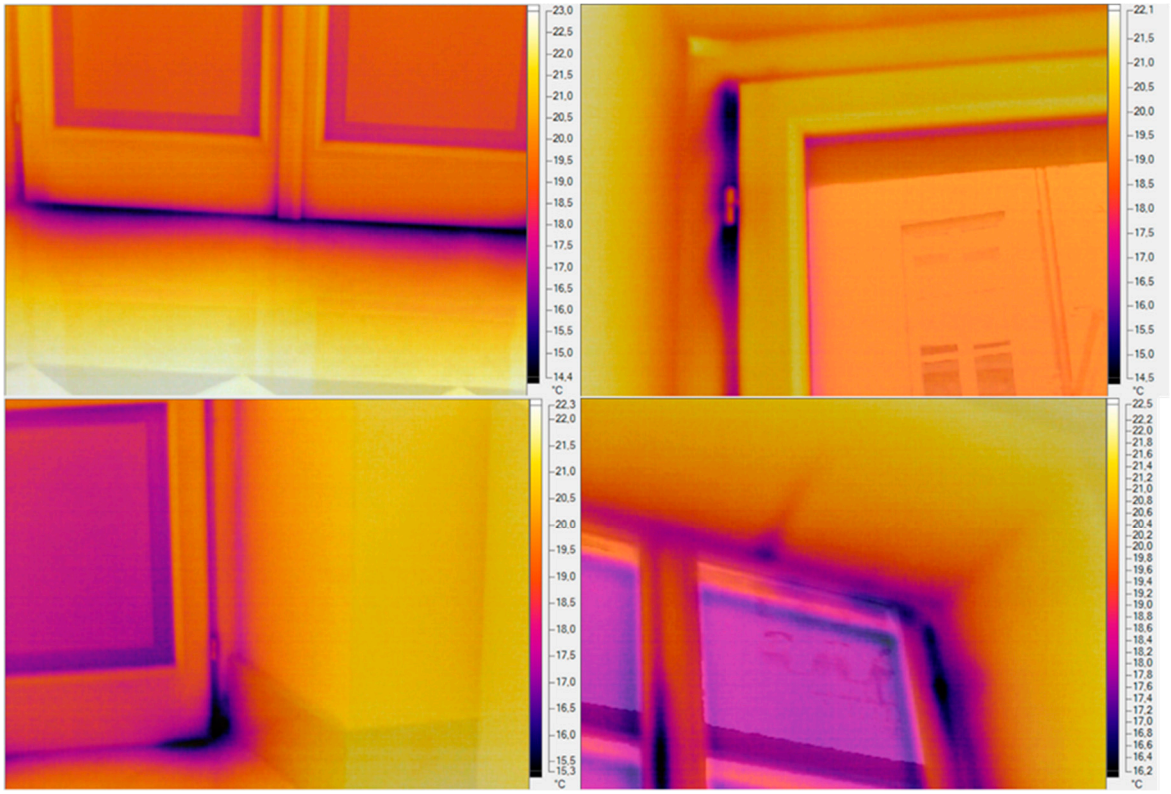

Figure 13. Example of installation errors on the windows.

The second problem encountered during the thermographic survey is that of reflected radiation.

The thermographic image must therefore be corrected by "balancing" the energy radiated from the surface of the wall with the component reflected from the surroundings that does not belong to the wall. While this is easy indoors, it gets complicated outdoors, where the sky ranges from −30 °C to +6 °C. So, particular attention was paid to the compensation of the reflected component of the energy radiated by the wall, although the surfaces studied have a high emissivity.

The compensation works as follows: by reducing the reflected temperature (background temperature), the surface temperature increases to compensate for the effect of cooling radiated from the environment to the surface. Conversely, the surface temperature decreases when the background temperature increases.

In this specific dense built heritage context, compensation was applied to the thermograms of the upper floors, because the reflected radiation comes from the sky.

The procedure follows these steps:

1. The thermogram is processed by setting the background temperature to the value of the sky (−30 °C in the absence of clouds). Temperature markers are placed on part of the façade (upper part). Figure 15a shows the measurement point;
2. The thermogram is post-processed by setting the reflected temperature to the value of the outdoor air temperature. Temperature markers are placed on part of the façade (lower part). Figure 15b shows the measurement point;
3. Figure 14 shows that, in the upper part of the façade, the mark indicates the temperature of the surface, which has been compensated with the value of the reflected temperature of the sky. In the lower part of the façade, the mark indicates the surface temperature, with the value of the background temperature set to the value of the ambient temperature. The colour palette on the right side of the images refers to a background temperature with the value of the ambient temperature. For this reason, in cases where the viewing angle becomes larger, to capture the upper parts of the façades (for which compensation with the temperature of the sky is required), the

temperature markings of the upper part of the façade do not correspond to the colour scheme of the image.

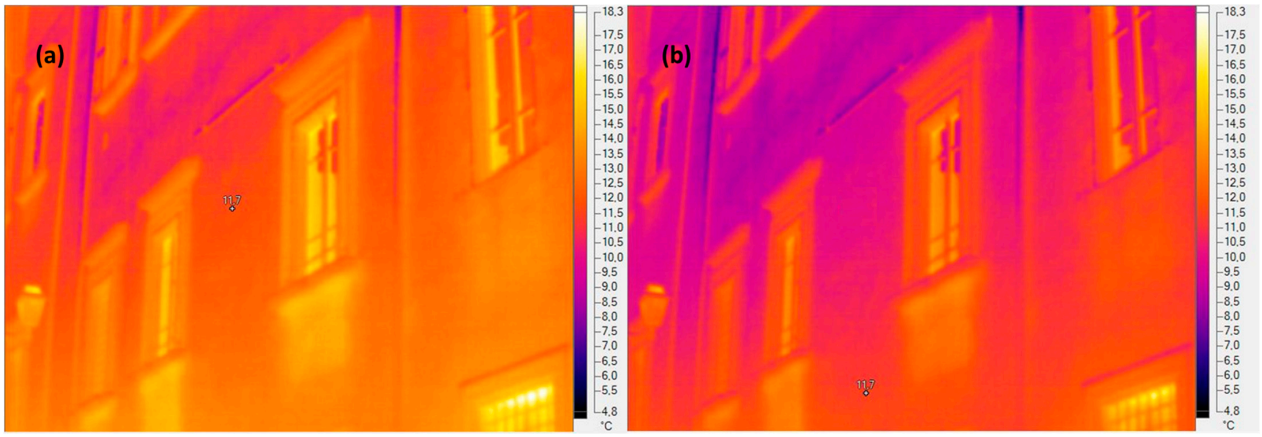

Figure 14. Vicolo del Divino Amore, Sector S1-1F/2F—ground floor (part), first floor, second floor (part): (**a**) temperature of the wall compensated at sky temperature, (**b**) temperature of the wall compensated at air temperature.

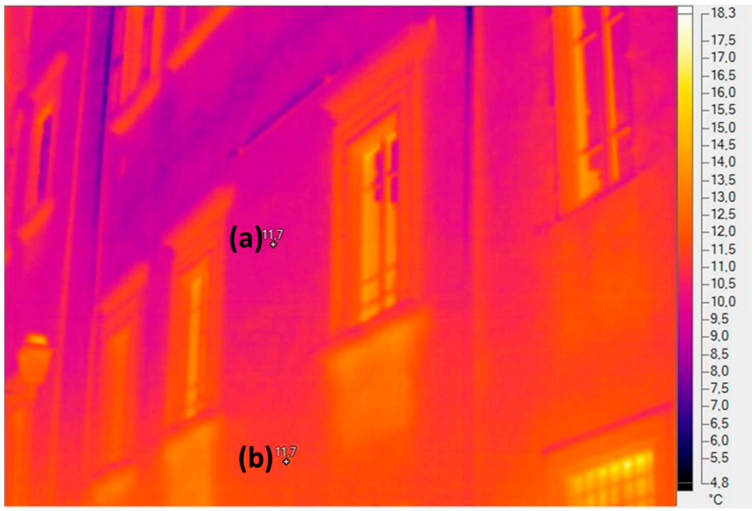

Figure 15. Vicolo del Divino Amore, Sector S1-1F/2F—ground floor (part), first floor, second floor (part): (**a**) background temperature at −30 °C (clear sky temperature), (**b**) background temperature at 11 °C (air temperature).

Applying the correct compensation, Figure 14 shows that the upper and lower parts of the wall have the same temperature, which means that the wall can be assumed to be uniform in construction.

A specific focus was placed on verifying the five-part layout hypothesised by the historical and architectural analysis and geometric survey. The investigation identified 11 potential stratigraphies (see Methodology), but did not find any differences in the horizontal development of the wall on the internal courtyard of Part-02, 03 and 04, as shown in Figure 16, discarding the heterogeneity initially assumed and reducing the parts from five to three.

Moreover, the thermographic measurement campaign showed that the presence of mouldings, both at external corners and in the area of the intermediate floors, did not reveal any thermal bridges in terms of shape (corners) or structure (intermediate floors).

On the contrary, several thermal bridges were identified at the intersection between the roofing and the façade of Via del Clementino and Vicolo del Divino Amore.

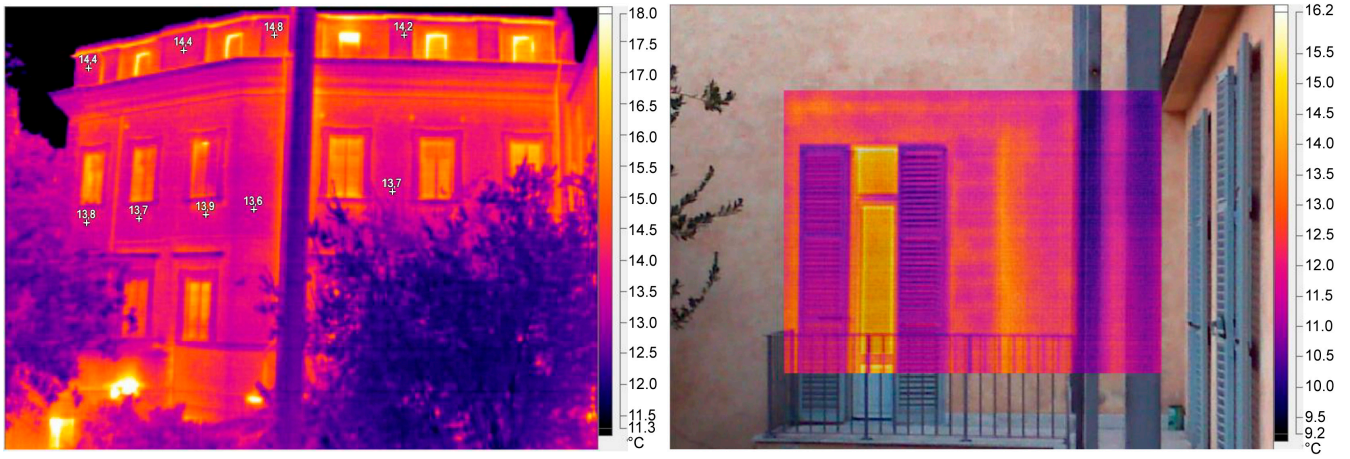

Figure 16. Example of thermographies used to analyse and discard the hypothesis of a distinction between Part-02, 03 and 04—Sector S9.

Another objective of the investigation was to detect anomalies in the building envelope.

Figure 16 (right side) shows a part of the main courtyard where it is possible to notice a non-uniform temperature on the right of the window, which initially allowed us to hypothesise either a junction between different buildings' construction systems (Part-03 and Part-04) or a previous window. The hint led to us deepening the historical investigation, and discovering that, in place of the current balcony, there was a closed 16th century loggia [119], page 24, which was probably accessed from a previous opening, recently closed. These findings strengthen the hypothesis that there is no distinction between the initially hypothesised Part-02, 03 and 04 of the building.

As already pointed out in Section 3.1, the thermographic survey led to a rough classification of the masonry types, allowing us to identify the most representative points where the HFM test should be carried out, and reduced the initially hypothesised five different construction systems to three (Part-01, Part-02-03-04 and Part-05). Moreover, HFM was used to confirm this updated hypothesis.

As an example, the differences in temperature, shown by the thermographic image corresponding to rooms 105 and 209, were tested with HFM to investigate if they could be ascribed to a reduction in the thickness of the same construction system or to two different wall construction types (see Table 4). Figure 17 shows the thermography results of points 5 and 6 of Figure 11.

Figure 17. Marker at the measuring points of the heat flow meter of rooms 105 (T = 9.4 °C) and 209 (T = 10.1 °C)—Sector S6-2F/3F.

Regarding the inside part of the building, no remarkable criticisms were found. It is worth mentioning that the thermography allowed us to check for wall irregularities before deploying each HFM point, identifying, for example, the location of the joists of the roof in room 318 and room 344 in order to place the sensors correctly, as shown in Figure 18.

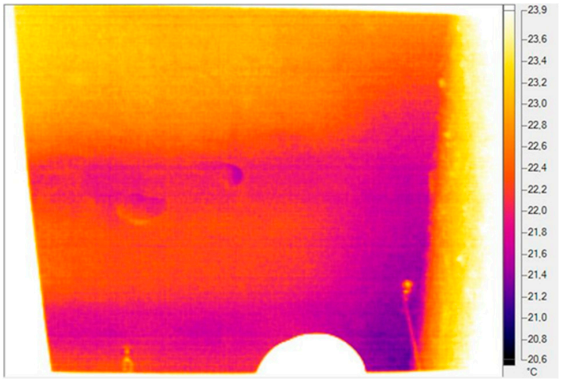

Figure 18. Third floor joist cold spots.

5.2. HFM

As pointed out in the previous section and also sketched in Figure 5, the joint findings of the historical and architectural analyses, of the geometric survey and the conservation state, double-checked by the IRT survey, led to a second and more refined hypothesis of three different construction systems, just two of which are historical (Part-01 and Part 02-03-04). This guided the choice of the walls' stratigraphies to investigate with HFM. The sunshine simulation of the building, undertaken to evaluate the contribution of solar irradiance to the walls during the period of the tests, supported the selection of measurement point locations with the best conditions (i.e., less sunshine during the measurement period). In addition, further checks were carried out with a thermal imaging camera from inside the building to avoid selecting a wall with defects. The heat flux meter was positioned on the internal surface of the wall to protect it from the weather and sunlight. The measurement campaign started by the end of January, when there were large temperature differences between the indoor and outdoor environments (about 10 °C) and consequently high thermal flux. So, the output signals of the sensors were higher and the system was less sensitive to external disturbances. The campaign was scheduled to have at least three days of data per measurement point, as required by Italian Regulation UNI ISO 9869-1:2015 [53]. However, before switching to a new location, the data were analysed to check if the trend of the progressive average of the conductance was sufficiently stable, and, if not, the instrument was kept in place for another round. The measurement points with the least sunshine (lower floors or north exposure) required the minimum measurement time.

As an example, Figure 19 reports the trends of the internal and external wall temperatures, shown together with the heat flow measured in room 220 during the measurement campaign.

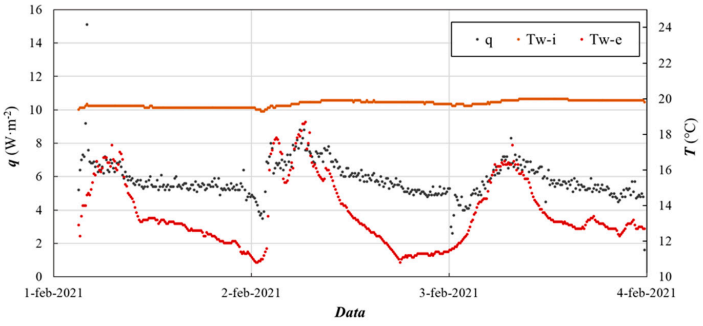

Figure 19. Trend of the temperature of the inner surface of the masonry (Tw-i), the outer surface (Tw-e) and the heat flow for room 220 (Meas. #1).

The application of the progressive average method resulted in the wall conductance being identified as an asymptotic value, characterised by the progressive average trend shown in Figure 20.

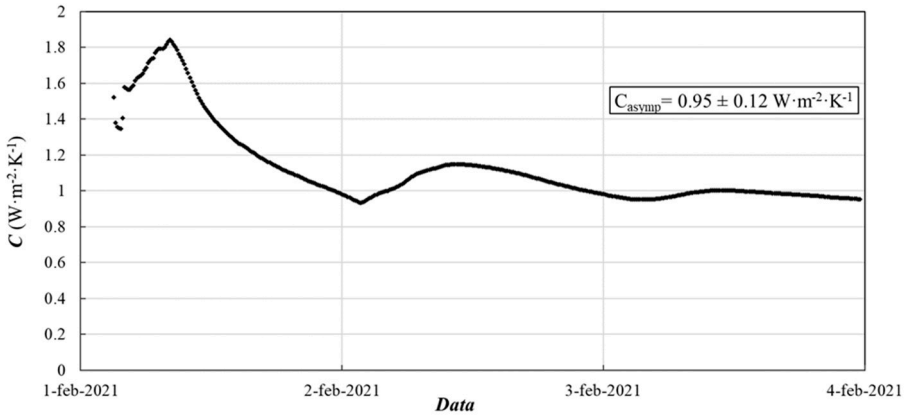

Figure 20. Trend of the progressive average of the conductance (C).

The uncertainty associated with the measurements was calculated by considering the error propagation of (1), taking into account the uncertainty of the heat flux equal to 5% of the measurement, as specified by the manufacturer, and the uncertainty of the temperature measurement equal to ±0.5 °C. The coverage factor k was assumed to be 1.

The heat transfer coefficient U given in Table 6 was calculated by starting from the measurement of C and taking into account the thermal resistances of the internal and external surfaces given in the UNI EN ISO 6946:2018 standard [129].

Table 6. Results of the thermofluximetric measurements taken with the progressive average method.

Orientation	Date (From–To)	Room #	Meas. #	C ($W \cdot m^{-2} \cdot K^{-1}$)	U_{calc} ($W \cdot m^{-2} \cdot K^{-1}$)	Convergence
NORTH-EAST	1 February 10:03–5 February 8:35	220	1	0.95 ± 0.12	0.82	YES
NORTH-EAST	5 February 10:59–9 February 8:39	116	2	0.81 ± 0.10	0.71	NO
EAST	9 February 10:45–16 February 8:40	127	3	0.56 ± 0.05	0.51	YES
EAST	16 February 11:02–23 February2 8:47	234	4	1.10 ± 0.11	0.92	YES
NORTH-WEST	23 February 10:43–26 February 7:53	105	5	0.62 ± 0.08	0.56	YES
NORTH-WEST	26 February 10:38–2 March 8:14	209	6	0.71 ± 0.07	0.63	YES
SOUTH-Internal Cloister	2 March 10:48–9 March 02:08	318	7	1.28 ± 0.14	1.05	YES
ROOF	10 March 11:19–11 March 14:19	318	8	1.06 ± 0.09	0.91	YES
ROOF	31 March 6:21–1 April 5:51	207	9	0.74 ± 0.07	0.66	NO

As described in Section 3.3, the inverse method was applied to double-check the HFM method results and further investigate the thermal properties of the material layers of the walls.

This simulation comparison in the dynamic regime, with optimisation by genetic algorithms, enabled us not only to consolidate the study of the thermal conductivity of the materials, but also to obtain rather high values for the density and specific heat of the internal fills considered as an unknown layer. These values allow for a double interpretation: on the one hand, they could indicate that the legislation tends to underestimate the thermal inertia values of real materials; on the other hand, they could be due to a compensatory effect of the model, which does not take into account the influences of the environmental parameters on the measurements, such as the effect of solar radiation.

Table 7 shows the thermal conductance values measured with HFM and the values resulting from the optimisation process described above.

Table 7. Conductance and transmittance measured and obtained by optimizing unknown stratigraphies with dynamic simulation software.

Wall Package Simulation (IDA ICE)		Meas #		C ($W \cdot m^{-2} \cdot K^{-1}$)				U_{calc} ($W \cdot m^{-2} \cdot K^{-1}$)			
	Data	Room		Meas.	Sim.	MAE	NMAE (%)	Meas.	Sim.	MAE	NMAE (%)
East	1 February 10:03–5 February 8:35	220	1	0.953	0.922	0.032	3.4	0.820	0.797	0.024	2.9
	5 February 10:59–9 February 8:39	116	2	0.806	0.803	0.003	0.4	0.709	0.706	0.003	0.4
	9 February 10:45–16 February 8:40	127	3	0.560	0.630	0.071	11	0.511	0.569	0.058	10
	16 February 11:02–23 February 8:47	**234**	**4**	**1.097**	**1.360**	**0.263**	**19**	**0.925**	**1.105**	**0.180**	**16**
North	23 February 10:43–26 February 7:53	105	5	0.621	0.635	0.014	2.1	0.562	0.573	0.011	1.9
	26 February 10:38–2 March 8:14	209	6	0.711	0.738	0.027	3.6	0.634	0.656	0.021	3.3
South	2 March 10:48–9 March 02:08	318	7	1.281	1.268	0.013	1.0	1.052	1.043	0.009	0.8

A general agreement is observed between the measured and simulated data, with a percentage deviation within 10%, leading us to confirm the measurement of room 116, which, despite not having convergence on the measurement, fell within the hypothesised construction typologies of the building, and excluding the measurement of room 234 (in bold), which, despite the convergence of the measurements, was not consistent with the masonry typologies identified, and resulted in a deviation of 19% in the value of U.

At the end of the investigation process, integrating the results of all the analyses carried out, the HFM analyses provided further support to the hypothesis of three main construction systems of the building with variable thicknesses (as shown in Figure 21), related to the three main parts identified: Part-01 is mainly load-bearing rubber masonry with a tuff wall layer and plaster on both sides, while Part-02-03-04 is tuff masonry with plaster on both sides, and Part-05 is hollow masonry and relates to recent interventions. Floors are confirmed to be steel beams with segmented hollow brick vaults for the inner floors, and the flat roofs are mostly arranged in an iron beam structure with hollow bricks, with lightened screed in the expanded clay (with few wooden structure exceptions). The HFM measurement number 9 was confirmed by a technical drawing retrieved after the analyses. For sloped roofs, both wooden and steel structure technologies are present.

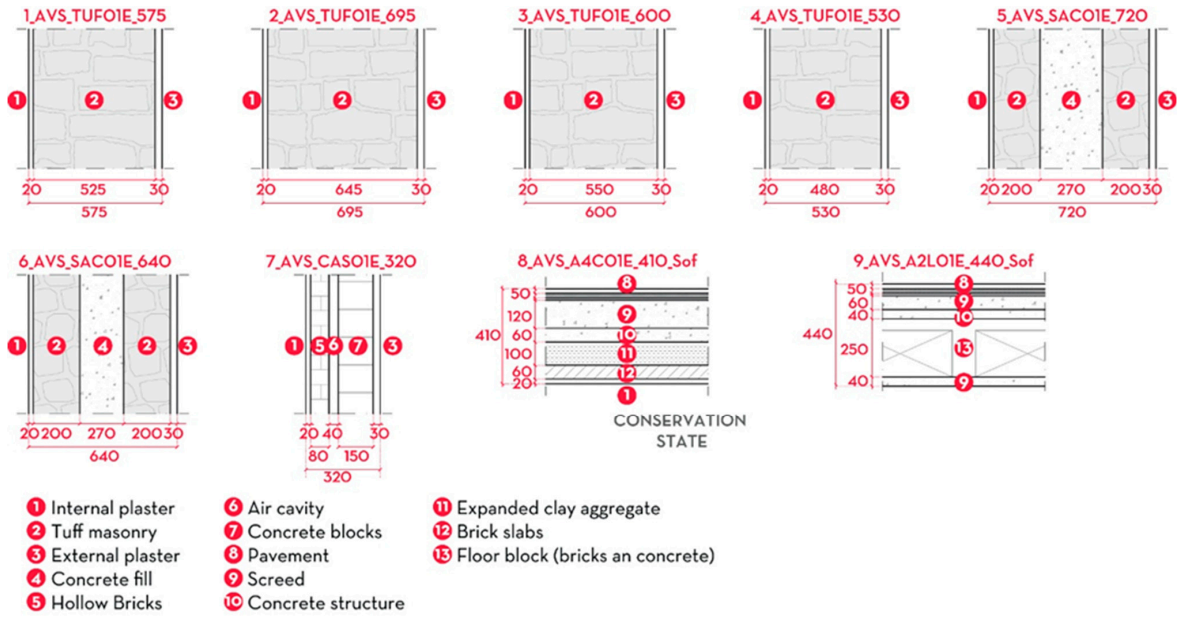

Figure 21. Specific technical sections representing the 9 identified wall types.

5.3. Microclimate Monitoring

The microclimate monitoring, as previously mentioned, covered a time span of 365 days, from the 1 January to the 31 December 2021.

The measurement of internal microclimatic variables was integrated with meteorological data provided by the ESTER laboratory of the University of Rome Tor Vergata, which is not far from the site under study. In Figure 22, the carpet plots of the Temperature, Relative Humidity (RH) and Global Horizontal Irradiance (GHI) for the whole period are reported.

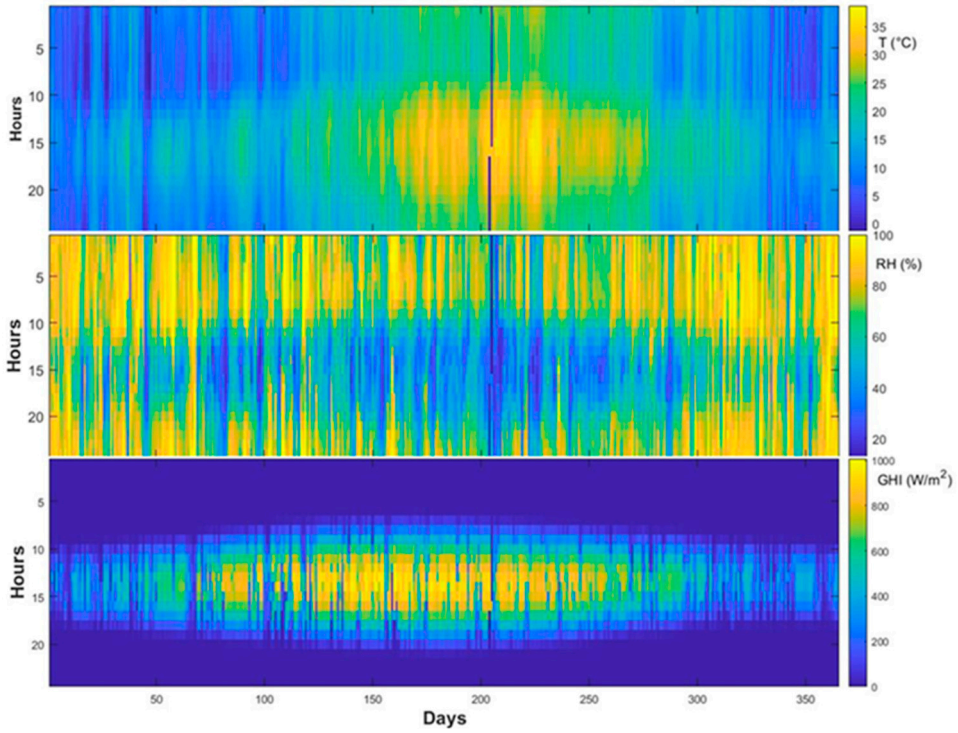

Figure 22. Temperature, Relative Humidity and Global Horizontal Irradiance for Tor Vergata area.

From the figure, it can be seen that 2021 was characterised by temperatures that were not too low in winter and mild in spring, while in summer they were quite high both during the day and at night. RH was quite high, especially during the night. Looking at the GHI, we can see that there was an interval of good weather in the central hours of the day for a period between the end of March and the first half of September.

The data collected during the whole year were divided into four periods, according to the operation of the heating/cooling system, as follows:

1. "Heating" from the 1 January to the 15 April and from the 1 November to the 31 December;
2. "1st IP" (First Intermediate Period) from the 16 April to the 20 June;
3. "Cooling" from the 21 June the 26 September;
4. "2nd IP" (Second Intermediate Period) from the 27 September to the 30 October.

Figure 23 shows a box plot of the data from the four periods, while Figure 24 shows a histogram of the selected rooms.

It can be observed that, during the winter period (heating), the median is in the middle of the box, both for the temperature and the relative humidity, indicating a normal distribution (see also the histograms in Figure 24). For all rooms, there are outliers both at high and low temperature. As far as temperature is concerned, we can notice that room sensors 3, 4, 5, 6 and 8 have many outliers at low temperature, which could be due to frequent window openings in the early morning, as can be observed from the temporal series of the data. Room sensor 1 (office reception), instead, has an almost identical number

of outliers at low and high temperatures, due to the high attendance of the room (opening and closing of the entrance door), the simultaneous presence of a few people, and the presence of one additional split to support the existing system.

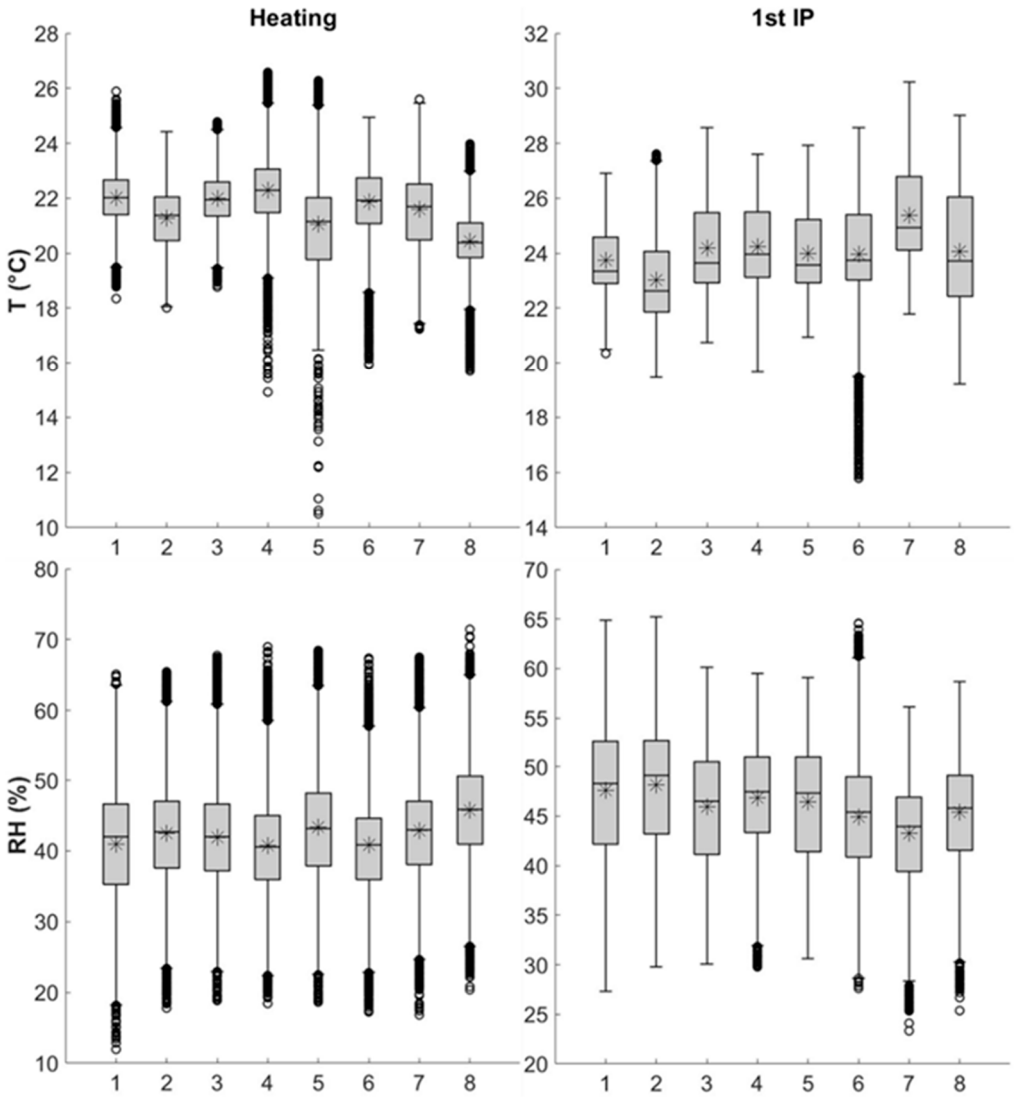

Figure 23. Carpet plot of temperature and relative humidity for the 8 rooms and external conditions, * symbol is the average value while the circles are the outliers.

The temperature variability (50% of the data contained in the box) is limited between 1 and 1.5 °C for all rooms (including night-time and weekends), except for room sensor 5, in room 105, which is usually unoccupied, with the fan coil usually turned off.

In the summer period (Cooling), we can notice a similar behaviour to the winter period, with very short boxes and the presence of numerous outliers. In this case, the outliers at low temperatures are mainly due to the low attendance of the room, while the ones at higher temperatures are due to a high attendance of the room and/or window openings.

In the two intermediate periods, it can be seen how the range of variability of the data (height of the whiskers) increases, and how the size of the boxes increases. In these two periods, the median is no longer in the middle of the box, and the distribution is no longer symmetric but bimodal, as can be seen in Figure 24.

We can identify two different trends. For the first IP, the second peak of the bimodal distribution is much lower than the first, or is almost absent; this may mean that the heat gain due to the presence of people or outdoor conditions is negligible, as the windows

are often open. On the contrary, in the second intermediate period, both peaks are clearly distinguishable; in this case, the lower frequency of the opening of windows does not compensate for the heat gain.

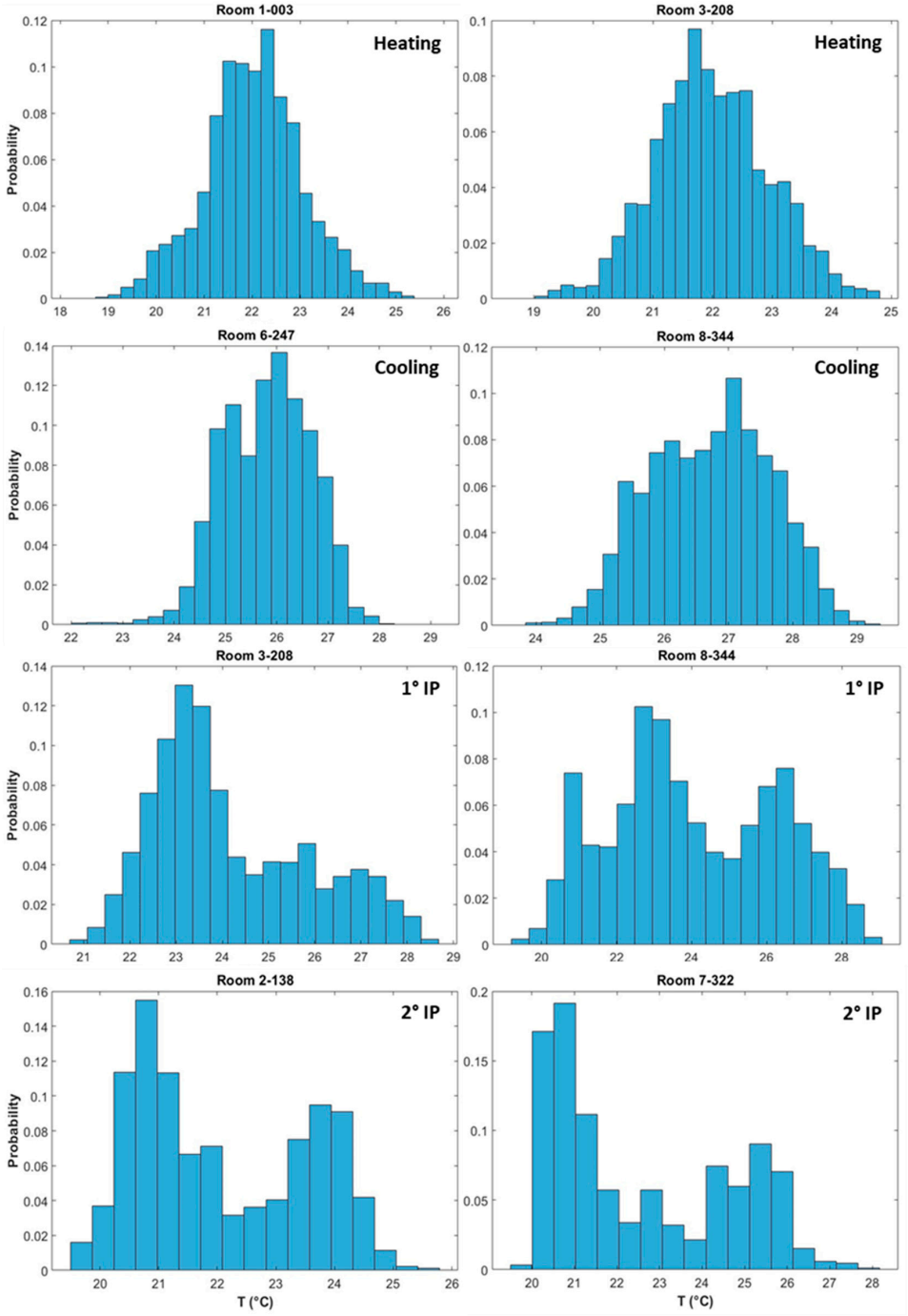

Figure 24. Temperature histograms of selected rooms.

The data (hourly average) of temperature and relative humidity are reported on a psychrometric chart, together with the seasonal average. The comfort zones (according to Italian regulation [130]) are also represented on the psychrometric chart for both the winter period ($20 \leq T \leq 22$ °C and $40 \leq RH \leq 60\%$) and the summer period ($24 \leq T \leq 26$ °C and $40 \leq RH \leq 60\%$).

Figure 25 shows the results for two rooms, number 138 (best comfort performance) and 209 (worst comfort performance).

Room 138's seasonal average is in the comfort zone, but is much shifted towards the lower limit in winter and the higher end in summer, indicating the presence of many points of discomfort. For all the other rooms, such as room 209 in Figure 25, it can be noted that in summer (Cooling) and winter (Heating), they are hardly ever in comfort conditions; this is better highlighted by the seasonal average, which falls outside the comfort limits. Finally, it should be noted that, for the heating period, the data appear highly dispersed, denoting a high variability in the microclimate, while in the cooling period, the data appear more concentrated with less variability. This is mainly due to the absence of relative humidity controls in the thermal system.

In order to evidence the behaviour of each room during the heating and cooling periods, the temperature trend of a typical day of heating (HDT) and cooling (CDT) was calculated. Each hourly value of the temperature for each room was averaged over the heating and cooling period. Figure 26 shows the HDT and CDT of two rooms. Rooms 322 and 344 were chosen, as they have a high density of occupancy with constant use throughout the year.

To create the HDT and CDT, the data were split into two groups by separating Working Days (WD) from Non-Working Days (NWD). This allowed us to highlight, on one hand, the contribution of people to the thermal load, and on the other hand, the average daily variation in the observed period.

In Figure 26 we can see that, if we take into account only the NWD, in the HDT, the two rooms have an almost constant temperature trend, with a daily thermal range of about 0.4 °C, slightly higher than the uncertainty of the measuring sensor (0.3 °C). Looking at CDT, on the other hand, on NWD, there is a more marked variability than in HDT (about 1.0 °C).

Comparing WD with NWD (when the thermal plant should be off for at least 36 h), both for the HDT and the CDT, between midnight and 8:00 am, we can notice the same temperature trend. From the data described above, and especially from the construction techniques used for rooms 322 and 344 (light hollow-brick masonry) and exposure (third floor, with three out of six sides exposed to the outside environment), we can conclude that thermal inertia cannot be solely responsible for such a small temperature difference between WD and NWD. So, we can deduce that the system (which, due to a series of unrepaired breakdowns, is currently serviced by an underpowered generator) is in operation 24 h a day, as also confirmed by energy bills and subsequent simulative analyses.

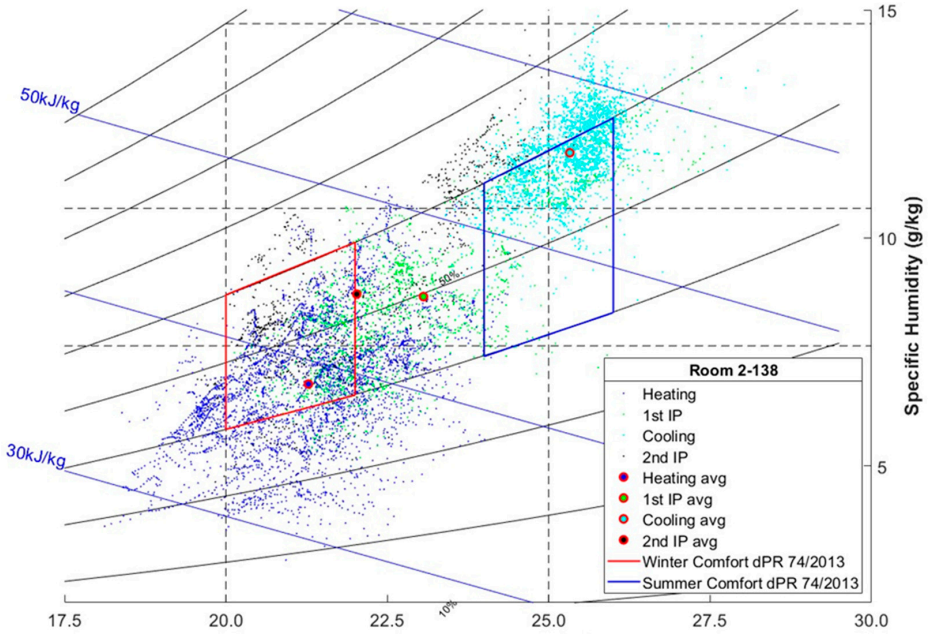

Figure 25. *Cont.*

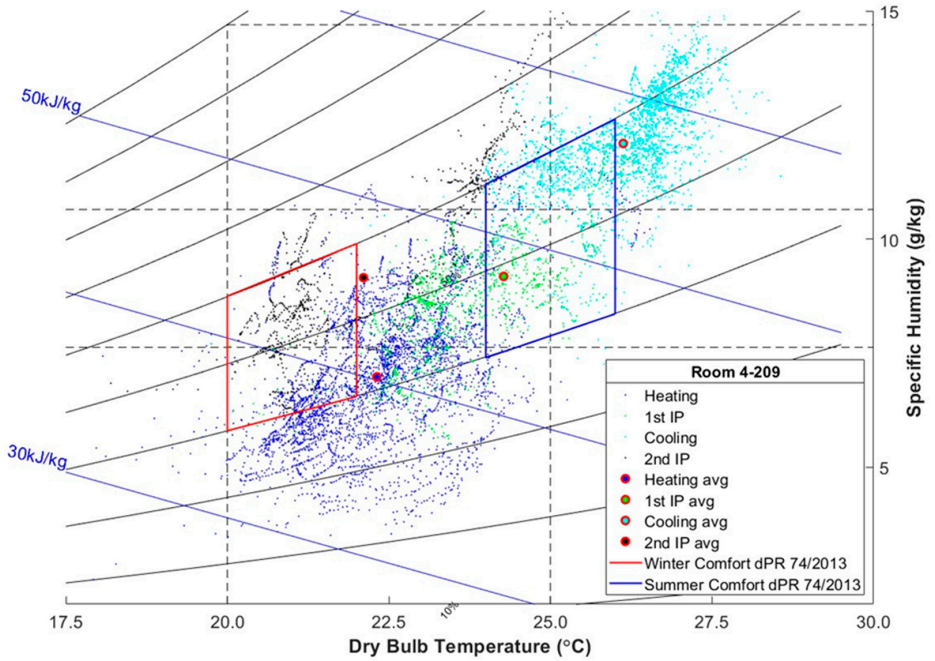

Figure 25. Room 138 and 209 psychrometric chart.

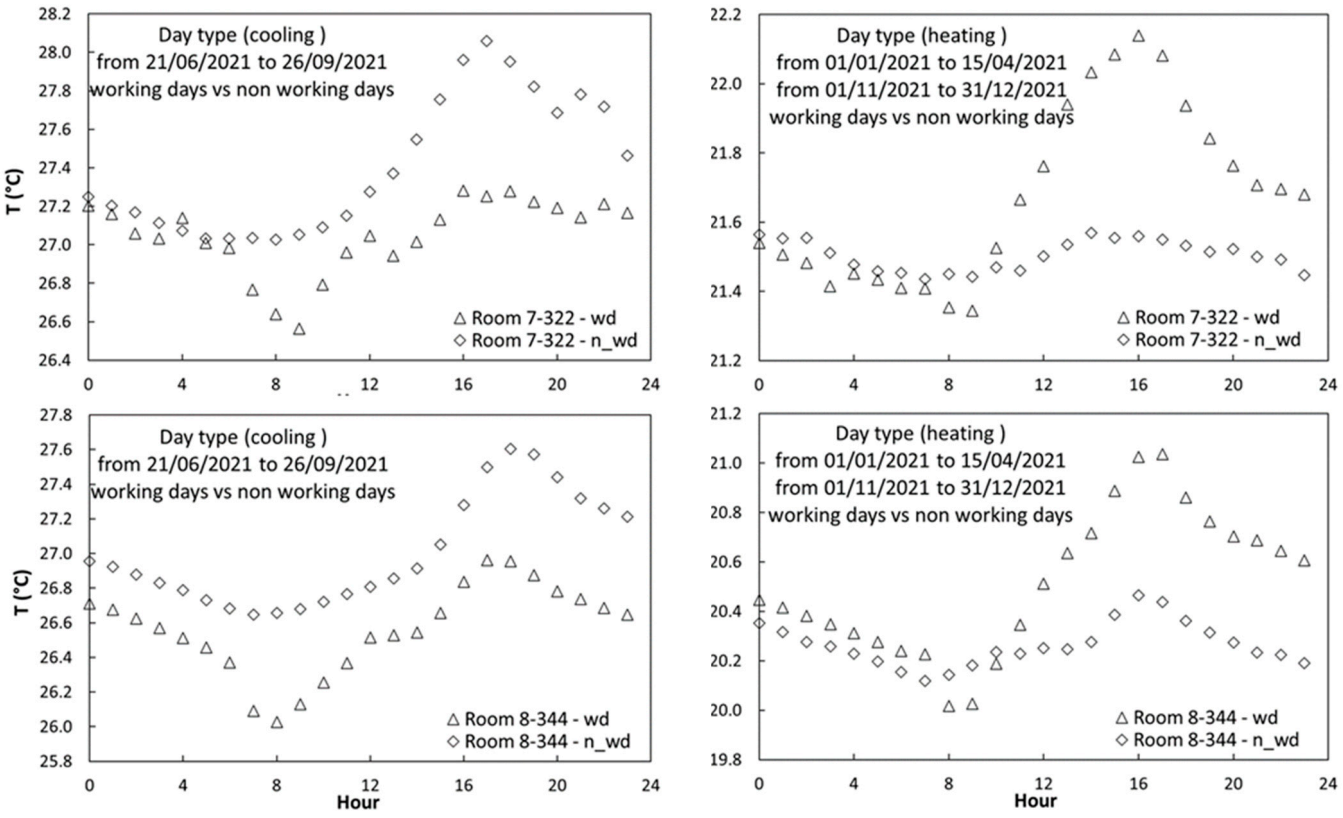

Figure 26. Day type of rooms 322 and 344.

Under this assumption, considering the WD of the HDT, we can notice the contribution of the presence of employees to the heating of the room, which results in a temperature peak around 4:00–5:00 p.m. due to heat accumulation.

For both HDT and CDT, we can also note that there is a drop in temperature at 8:00 a.m. in the trend of the WD, not visible in the trend of NWD. This drop may be due

to either the regular opening of the windows by the cleaning staff or by the employees when they arrive. However, opening the windows on WD decreases the average hourly temperature compared to NWD.

5.4. HBIM Integration

Graphisoft Archicad 26 was chosen as the BIM authoring software. Within the chosen HBIM approach, all the data gathered from the analysis phase, according to a preset template [131], were uploaded to a CDE, which includes a robust file repository of 100 Gb, on a local ad-hoc server with controlled access via the internet that guarantees traceability, security, accessibility and version history for all the files. Given the heterogeneity of the information collected, comprising alphanumeric data, reports, images, drawings, tables, etc., the CDE allows for direct integration into the 3D HBIM model, if possible and/or feasible, or at least its structured organisation and link to the model. For example, the thermophysical properties of materials were integrated directly into the BIM model; fenestration parameters needed to be calculated in the BPS model, and so some of the data were transferred through the interoperability process (windows main dimensions and typology), while other in-depth data (concerning frame, inlets, boxes etc.) were extracted from BIM through a spreadsheet and then manually inputted in the model.

A naming convention was developed to be used for the content of all documents uploaded to a CDE and all objects within BIM and BPS models, in line with ISO 19650-1:2018 [87] and coherent with the BIM software identification system; in this way, the same elements in all the files of the CDE are referenced with the same unique code. Following the naming convention, a summary table of data collected in the CDE was used as the reference point for data consistency between the HBIM model and the energy model, especially for the connection of data related to abstract elements such as thermal zones (present only in the energy model) and rooms (present in the HBIM model and the energy model).

6. Conclusions

The main contribution of this paper is the proposal of an integrated methodology that involves historical and architectural analyses, geometric surveys and conservation state analyses, together with in situ non-destructive techniques, implemented in an HBIM environment, to acquire an accurate representation of a historical building that will support dynamic simulation modelling.

Specifically, the thermographic analysis allowed us to support the characterization of the envelope, also identifying thermal bridges of form and structure and giving insights into different construction materials and discontinuities, thus helping both the classification of masonry types and the tailoring of HFM analyses. The main challenges faced concerned the narrow streets surrounding the buildings, which hinder the ideal shooting distances and angles, and the reflected radiation. The analysis thus required a specific correction to balance the energy radiated from the walls with the component reflected from the surroundings, especially for the sky.

The HFM analysis allowed us to double-check the hypothesis on the building's construction systems up to their thermophysical characterisation. Despite the precautions taken in keeping the sensor on for several days and selecting the least sun-exposed surfaces, the heterogeneities and complexities of the case study increased the difficulties in performing reliable HFM measurements. For this reason, an iterative procedure, integrating different approaches (norms, HFM method, inverse method with dynamic modelling), was implemented. The approach can be helpful in cases, such as ours, in which destructive tests are not allowed, time is limited, access to the building is restricted, and no ideal configuration for the HFM is possible.

Long-term and extensive indoor environmental monitoring, besides being essential for the conservation risk and thermal comfort evaluation, allowed us to study the environmental behaviour of the building, and to spot a limited temperature variability and widespread discomfort condition in summer that led to further analyses of the operational

schedules of the HVAC system. Specific studies on a typical day of heating and cooling, and a comparison between working and non-working days, showed a 24 h operation, as confirmed also by the energy bills. These studies also provided additional hints of the building's active and passive behaviour and the occupancy patterns, to be addressed in the subsequent simulations and which support the design of interventions.

Finally, the HBIM-based approach played the role of an interdisciplinary facilitator, allowing the coherent management of the analyses within a wider building information process, despite the challenges due to the high heterogeneity of data, especially when not directly linked to a specific building object in the HBIM model, and thus requiring strong support from a CDE. HBIM helped the interdisciplinary team to keep track of the development of the study by iteratively updating the models and the CDE, tuning the initial hypotheses as the data were acquired and new hypotheses were consolidated.

Overall, the main limitation of the methodology concerns the high skill level required by its operators that still hampers its technological transfer to professional practice, despite the growing need for processes and datasets to support the energy and environmental improvement of historical buildings. Nevertheless, the work done and the results gained suggest some important aspects that the researchers and practitioners could take into account when approaching a similar endeavour:

- the relevance of the careful planning of in situ activities and of preliminary supporting simulations to optimise time and cost, in synergy with the actors of the process;
- the crucial value of experts from all the different disciplines working together, both in the survey and measurement phase, as well as in the data elaboration phase, to achieve better results.

Author Contributions: Conceptualization, C.C., G.B., F.C., L.M. and E.G.; methodology, C.C., G.B., F.C., L.M. and E.G.; validation, C.C. and G.B.; formal analysis, C.C. and G.B.; investigation, C.C., G.B., F.C. and L.M.; resources, C.C., F.C. and E.G.; data curation, G.B., F.C. and L.M.; writing—original draft preparation, C.C., G.B., F.C. and L.M.; writing—review and editing, C.C., G.B., F.C., L.M. and E.G.; visualization, G.B. and L.M.; supervision, E.G.; funding acquisition, F.C. and E.G. All authors have read and agreed to the published version of the manuscript.

Funding: This research was funded within the activities of BEEP project (BIM for Energy Efficiency in the Public sector) funded under the ENI CBC Med programme grant contract N° 27/1243 of 5 August 2019.

Institutional Review Board Statement: Not applicable.

Informed Consent Statement: Not applicable.

Data Availability Statement: The data presented in this study are available on request from the corresponding author.

Acknowledgments: The authors would like to thank the experts and managers involved in the process: Alessandro Mengoli, Leo Lorenzi, Angelo Limiti; the technical office of the Legal Council of State (Avvocatura di Stato) and the State Property Agency (Agenzia del Demanio). The data loggers were supplied by Tecnoel Srl, which also took care of their calibration in a climatic chamber.

Conflicts of Interest: The authors declare no conflict of interest.

Nomenclature

Latin		
A	surface	[m^2]
c_p	specific heat	[$J \cdot kg^{-1} \cdot K^{-1}$]
C	conductance	[$W \cdot m^{-2} \cdot K^{-1}$]
$\dot{q}$	heat flux for unit area	[$W \cdot m^{-2}$]
$\dot{Q}$	thermal radiation power	[W]
T	temperature	[K or °C]
U	heat transfer coefficient	$W \cdot m^{-2} \cdot K^{-1}$]
Greek		
λ	thermal conductivity	$W \cdot m^{-1} \cdot K^{-1}$]
ε	emissivity	
ρ	density	[$kg \cdot m^{-3}$]
σ	Stefan–Boltzmann constant	$W \cdot m^{-2} \cdot K^{-4}$]
Subscripts		
calc	calculated	
e	external	
i	internal	
meas	measured	
r	reflected	
w	wall	
Abbreviation		
BIM	Building Information Modelling	
BPS	Building Performance Simulation	
CDE	Common Data Environment	
CDT	Cooling Day Type	
GHI	Global Horizontal Irradiance	
HBIM	Heritage Building Information Modelling	
HDT	Heating Day Type	
HFM	Heat Flow Meter	
HVAC	Heating Ventilation Air Conditioning	
IP	Intermediate Period	
IRT	Infrared Thermography	
NDT	Non-Destructive Techniques	
NWD	Non-Working Days	
RH	Relative Humidity	
WD	Working Days	

References

1. Eurostat, Census Hub HC53. 2011. Available online: https://ec.europa.eu/CensusHub2/query.do?step=selectHyperCube&qhc=false (accessed on 13 January 2023).
2. European Commission. Proposal for a Directive of The European Parliament and of the Council on the Energy Performance of Buildings (Recast). 2021. Available online: https://eur-lex.europa.eu/legal-content/EN/TXT/?uri=CELEX%3A52021PC0802&qid=1641802763889 (accessed on 9 September 2022).
3. European Commission. Energy Performance of Buildings Directive. 2018. Available online: https://energy.ec.europa.eu/topics/energy-efficiency/energy-efficient-buildings/energy-performance-buildings-directive_en (accessed on 13 January 2023).
4. Staniaszek, D. (Ed.) *A Guide to Developing Strategies for Building Energy Renovation*; BPIE: Brussels, Belgium, 2013.
5. Economidou, M. (Ed.) *Europe's Buildings under the Microscope*; Buildings Performance Institute Europe: Brussels, Belgium, 2011.
6. European Commission. EU Buildings Factsheets. 2014. Available online: https://ec.europa.eu/energy/eu-buildings-factsheets_en (accessed on 9 September 2022).
7. European Parliament. Directive (EU) 2018/844 of the European Parliament and of the Council of 30 May 2018 Amending Directive 2010/31/EU on the Energy Performance of Buildings and Directive 2012/27/EU on Energy Efficiency (Text with EEA Relevance). 2018. Available online: http://data.europa.eu/eli/dir/2018/844/oj/eng (accessed on 9 September 2022).
8. European Parliament. Directive 2010/31/EU of the European Parliament and of the Council of 19 May 2010 on the Energy Performance of Buildings (Recast). 2010. Available online: http://data.europa.eu/eli/dir/2010/31/oj/eng (accessed on 9 September 2022).

9. European Parliament. Directive 2012/27/EU of the European Parliament and of the Council of 25 October 2012 on Energy Efficiency, Amending Directives 2009/125/EC and 2010/30/EU and Repealing Directives 2004/8/EC and 2006/32/EC Text with EEA Relevance. 2012. Available online: http://data.europa.eu/eli/dir/2012/27/oj/eng (accessed on 9 September 2022).
10. SECHURBA Project. Sustainable Energy Communities in Historic Urban Areas. 2008. Available online: https://ec.europa.eu/energy/intelligent/projects/sites/iee-projects/files/projects/documents/sechurba_guide_en.pdf (accessed on 9 September 2022).
11. Gigliarelli, E.; Calcerano, F.; Cessari, L. Analytic Hierarchy Process. A Multi-Criteria Decision Support Approach for the Improvement of the Energy Efficiency of Built Heritage. In Proceedings of the EEHB2018 The 3rd International Confernece on Energy Efficiency in Historic Buildings, Tor Broström Lisa Nilsen Susanna Carlsten, Uppsala University, Department of Art History, Visby, Sweden, 26–28 September 2018. Available online: http://www.iea-shc.org/Data/Sites/1/publications/Energy-efficiency-in-historic-buildings_preliminary-conference-report.pdf (accessed on 9 September 2022).
12. JPICH. Strategic Research Agenda—JPI Cultural Heritage and Global Change. 2014. Available online: http://www.jpi-culturalheritage.eu/wp-content/uploads/SRA-2014-06.pdf (accessed on 9 September 2022).
13. JPICH. Strategic Research and Innovation Agenda 2020: Final Version of the Updated JPI CH SRIA Published. 2020. Available online: https://www.heritageresearch-hub.eu/strategic-research-and-innovation-agenda-2020-sria/ (accessed on 8 October 2021).
14. Ballard, C.; Baron, N.; Bourgès, A.; Bucher, B.; Cassar, M.; Daire, M.-Y.; Daly, C.; Egusquiza, A.; Fatoric, S.; Holtorf, C.; et al. Cultural Heritage and Climate Change: New Challenges and Perspectives for Research. 2022. Available online: https://www.heritageresearch-hub.eu/white-paper-cultural-heritage-and-climate-change-new-challenges-and-perspectives-for-research/ (accessed on 5 April 2022).
15. Troi, A.; Bastian, Z. *Energy Efficiency Solutions for Historic Buildings a Handbook*; Birkhäuser: Basel, Switzerland, 2015.
16. Blumberga, A.; de Place, J.H. Ribuild: Written Guidelines for Decision Making Concerning the Possible Use of Internal Insulation in Historic Buildings. 2020. Available online: https://static1.squarespace.com/static/5e8c2889b5462512e400d1e2/t/5f04215c5b6cfa0aa7baa5b1/1594106230146/Written+guidelines+for+decision+making+concerning+the+possible.pdf (accessed on 9 September 2022).
17. Kilian, R.; Leissner, J.; Antretter, F.; Holl, K.; Holm, A. Modeling Climate Change impact on Cultural Heritage—The European Project Climate for Culture. In Proceedings of the COST C26 Action Final Conference, Naples, Italy, 16–18 September 2010.
18. Eriksson, P.; Hermann, C.; Hrabovszky-Horváth, S.; Rodwell, D. EFFESUS Methodology for Assessing the Impacts of Energy-Related Retrofit Measures on Heritage Significance, Hist. *Environ. Policy Pract.* **2014**, *5*, 132–149. [CrossRef]
19. Andreotti, M.; Bottino-Leone, D.; Calzolari, M.; Davoli, P.; Pereira, L.D.; Lucchi, E.; Troi, A. Applied Research of the Hygrothermal Behaviour of an Internally Insulated Historic Wall without Vapour Barrier: In Situ Measurements and Dynamic Simulations. *Energies* **2020**, *13*, 3362. [CrossRef]
20. Akkurt, G.G.; Aste, N.; Borderon, J.; Buda, A.; Calzolari, M.; Chung, D.; Costanzo, V.; Del Pero, C.; Evola, G.; Huerto-Cardenas, H.E.; et al. Dynamic thermal and hygrometric simulation of historical buildings: Critical factors and possible solutions, Renew. *Sustain. Energy Rev.* **2020**, *118*, 109509. [CrossRef]
21. Heritage, E.W. Energy Heritage. A Guide to Improving Energy Efficiency in Traditional and Historic Homes. 2008. Available online: http://www.changeworks.org.uk/resources/energy-heritage-a-guide-to-improving-energy-efficiency-in-traditional-and-historic-homes (accessed on 9 September 2022).
22. MIBACT, Linee Di Indirizzo Per Il Miglioramento Dell'efficienza Energetica Nel Patrimonio Culturale. Architettura, Centri e Nuclei Storici Ed Urbani. 2015. Available online: http://www.beap.beniculturali.it/opencms/multimedia/BASAE/documents/2015/10/27/1445954374955_Linee_indirizzo_miglioramento_efficienza_energetica_nel_patrimonio_culturale.pdf (accessed on 9 September 2022).
23. Carbonara, G. Energy efficiency as a protection tool. *Energy Build.* **2015**, *95*, 9–12. [CrossRef]
24. Gigliarelli, E.; Calcerano, F.; Cessari, L.; Bim, H. Numerical Simulation and Decision Support Systems: An Integrated Approach for Historical Buildings Retrofit. *Energy Procedia* **2017**, *133*, 135–144. [CrossRef]
25. Potts, A. *European Cultural Heritage Green Paper*; Europa Nostra: Hague, The Netherlands, 2021.
26. Cornaro, C.; Puggioni, V.A.; Strollo, R.M. Dynamic simulation and on-site measurements for energy retrofit of complex historic buildings: Villa Mondragone case study. *J. Build. Eng.* **2016**, *6*, 17–28. [CrossRef]
27. Frasca, F.; Cornaro, C.; Siani, A.M. A method based on environmental monitoring and building dynamic simulation to assess indoor climate control strategies in the preventive conservation within historical buildings. *Sci. Technol. Built Environ.* **2019**, *25*, 1253–1268. [CrossRef]
28. Frasca, F.; Verticchio, E.; Cornaro, C.; Siani, A.M. Performance assessment of hygrothermal modelling for diagnostics and conservation in an Italian historical church. *Build. Environ* **2021**, *193*, 107672. [CrossRef]
29. Kilic, G. Using advanced NDT for historic buildings: Towards an integrated multidisciplinary health assessment strategy. *J. Cult. Herit.* **2015**, *16*, 526–535. [CrossRef]
30. Tejedor, B.; Lucchi, E.; Bienvenido-Huertas, D.; Nardi, I. Non-destructive techniques (NDT) for the diagnosis of heritage buildings: Traditional procedures and futures perspectives. *Energy Build.* **2022**, *263*, 112029. [CrossRef]
31. Lucchi, E. Applications of the infrared thermography in the energy audit of buildings: A review. *Renew. Sustain. Energy Rev.* **2018**, *82*, 3077–3090. [CrossRef]
32. Dias, I.S.; Flores-Colen, I.; Silva, A. Critical Analysis about Emerging Technologies for Building's Façade Inspection. *Buildings* **2021**, *11*, 53. [CrossRef]

33. Kylili, A.; Fokaides, P.A.; Christou, P.; Kalogirou, S.A. Infrared thermography (IRT) applications for building diagnostics: A review. *Appl. Energy.* **2014**, *134*, 531–549. [CrossRef]
34. Fox, M.; Goodhew, S.; De Wilde, P. Building defect detection: External versus internal thermography. *Build. Environ.* **2016**, *105*, 317–331. [CrossRef]
35. Kirimtat, A.; Krejcar, O. A review of infrared thermography for the investigation of building envelopes: Advances and prospects. *Energy Build.* **2018**, *176*, 390–406. [CrossRef]
36. Bisegna, F.; Ambrosini, D.; Paoletti, D.; Sfarra, S.; Gugliermetti, F. A qualitative method for combining thermal imprints to emerging weak points of ancient wall structures by passive infrared thermography—A case study. *J. Cult. Herit.* **2014**, *15*, 199–202. [CrossRef]
37. Paoletti, D.; Ambrosini, D.; Sfarra, S.; Bisegna, F. Preventive thermographic diagnosis of historical buildings for consolidation. *J. Cult. Herit.* **2013**, *14*, 116–121. [CrossRef]
38. Pescari, S.; Budău, L.; Vîlceanu, B. Rehabilitation and restauration of the main façade of historical masonry building –Romanian National Opera Timisoara. *Case Stud. Constr. Mater.* **2023**, *18*, e01838. [CrossRef]
39. Kilic, G. Assessment of historic buildings after an earthquake using various advanced techniques. *Structures* **2023**, *50*, 538–560. [CrossRef]
40. Cascardi, A.; Longo, F.; Perrone, D.; Lassandro, P.; Aiello, M.A. Thermography Investigation and Seismic Vulnerability Assessment of a Historical Vaulted Masonry Building. *Heritage* **2022**, *5*, 2041–2061. [CrossRef]
41. Avdelidis, N.P.; Moropoulou, A. Applications of infrared thermography for the investigation of historic structures. *J. Cult. Herit.* **2004**, *5*, 119–127. [CrossRef]
42. Valluzzi, M.R.; Lorenzoni, F.; Deiana, R.; Taffarel, S.; Modena, C. Non-destructive investigations for structural qualification of the Sarno Baths, Pompeii. *J. Cult. Herit.* **2019**, *40*, 280–287. [CrossRef]
43. Meola, C. Infrared Thermography in the Architectural Field. *Sci. World J.* **2013**, *2013*, 323948. [CrossRef] [PubMed]
44. Falchi, L.; Slanzi, D.; Balliana, E.; Driussi, G.; Zendri, E. Rising damp in historical buildings: A Venetian perspective. *Build. Environ.* **2018**, *131*, 117–127. [CrossRef]
45. Barbosa, M.T.G.; Rosse, V.J.; Laurindo, N.G. Thermography evaluation strategy proposal due moisture damage on building facades. *J. Build. Eng.* **2021**, *43*, 102555. [CrossRef]
46. Rosina, E.; Zala, M.; Ammendola, A. The moisture issue affecting the historical buildings in the Po valley: A case study approach. *J. Cult. Herit.* **2023**, *60*, 78–85. [CrossRef]
47. Trevisiol, F.; Barbieri, E.; Bitelli, G. Multitemporal Thermal Imagery Acquisition and Data Processing on Historical Masonry: Experimental Application on a Case Study. *Sustainability* **2022**, *14*, 559. [CrossRef]
48. Nardi, I.; de Rubeis, T.; Taddei, M.; Ambrosini, D.; Sfarra, S. The energy efficiency challenge for a historical building undergone to seismic and energy refurbishment. *Energy Procedia* **2017**, *133*, 231–242. [CrossRef]
49. De Berardinis, P.; Bartolomucci, C.; Capannolo, L.; De Vita, M.; Laurini, E.; Marchionni, C. Instruments for Assessing Historical Built Environments in Emergency Contexts: Non-Destructive Techniques for Sustainable Recovery. *Buildings* **2018**, *8*, 27. [CrossRef]
50. Bienvenido-Huertas, D.; Moyano, J.; Marín, D.; Fresco-Contreras, R. Review of in situ methods for assessing the thermal transmittance of walls. *Renew. Sustain. Energy Rev.* **2019**, *102*, 356–371. [CrossRef]
51. Teni, M.; Krstić, H.; Kosiński, P. Review and comparison of current experimental approaches for in-situ measurements of building walls thermal transmittance. *Energy Build.* **2019**, *203*, 109417. [CrossRef]
52. *ISO 6946:2007*; Building Components and Building Elements—Thermal Resistance and Thermal Transmittance—Calculation Method. 2007. Available online: https://www.iso.org/standard/40968.html (accessed on 9 September 2022).
53. *ISO 9869-1:2014*; Thermal Insulation—Building Elements—In-Situ Measurement of Thermal Resistance and Thermal Transmittance—Part 1: Heat flow Meter Method. 2014. Available online: https://www.iso.org/standard/59697.html (accessed on 9 September 2022).
54. Bienvenido-Huertas, D.; Rodríguez-Álvaro, R.; Moyano, J.J.; Rico, F.; Marín, D. Determining the U-Value of Façades Using the Thermometric Method: Potentials and Limitations. *Energies* **2018**, *11*, 360. [CrossRef]
55. Fokaides, P.A.; Kalogirou, S.A. Application of infrared thermography for the determination of the overall heat transfer coefficient (U-Value) in building envelopes. *Appl. Energy.* **2011**, *88*, 4358–4365. [CrossRef]
56. Dall'O', G.; Sarto, L.; Panza, A. Infrared Screening of Residential Buildings for Energy Audit Purposes: Results of a Field Test. *Energies* **2013**, *6*, 3859–3878. [CrossRef]
57. Albatici, R.; Tonelli, A.M. Infrared thermovision technique for the assessment of thermal transmittance value of opaque building elements on site. *Energy Build.* **2010**, *42*, 2177–2183. [CrossRef]
58. Meng, X.; Gao, Y.; Wang, Y.; Yan, B.; Zhang, W.; Long, E. Feasibility experiment on the simple hot box-heat flow meter method and the optimization based on simulation reproduction. *Appl. Therm. Eng.* **2015**, *83*, 48–56. [CrossRef]
59. Meng, X.; Luo, T.; Gao, Y.; Zhang, L.; Shen, Q.; Long, E. A new simple method to measure wall thermal transmittance in situ and its adaptability analysis. *Appl. Therm. Eng.* **2017**, *122*, 747–757. [CrossRef]
60. Lucchi, E. Thermal transmittance of historical brick masonries: A comparison among standard data, analytical calculation procedures, and in situ heat flow meter measurements. *Energy Build.* **2017**, *134*, 171–184. [CrossRef]

61. Lucchi, E. Thermal transmittance of historical stone masonries: A comparison among standard, calculated and measured data. *Energy Build.* **2017**, *151*, 393–405. [CrossRef]
62. Tejedor, B.; Casals, M.; Gangolells, M.; Roca, X. Quantitative internal infrared thermography for determining in-situ thermal behaviour of façades. *Energy Build.* **2017**, *151*, 187–197. [CrossRef]
63. Tejedor, B.; Barreira, E.; Almeida, R.M.S.F.; Casals, M. Automated data-processing technique: 2D Map for identifying the distribution of the U-value in building elements by quantitative internal thermography. *Autom. Constr.* **2021**, *122*, 103478. [CrossRef]
64. Ascione, F.; Ceroni, F.; De Masi, R.F.; Rossi, F.D.; Pecce, M.R. Historical buildings: Multidisciplinary approach to structural/energy diagnosis and performance assessment. *Appl. Energy.* **2017**, *185*, 1517–1528. [CrossRef]
65. Roque, E.; Vicente, R.; Almeida, R.M.S.F.; da Silva, J.M.; Ferreira, A.V. Thermal characterisation of traditional wall solution of built heritage using the simple hot box-heat flow meter method: In situ measurements and numerical simulation. *Appl. Therm. Eng.* **2020**, *169*, 114935. [CrossRef]
66. Baker, P. *U-Values and Traditional Buildings-In Situ Measurements and Their Comparisons to Calculated Values*; Technical Paper 10; Glasgow Caledonian University: Glasgow, UK, 2010.
67. De Berardinis, P.; Rotilio, M.; Marchionni, C.; Friedman, A. Improving the energy-efficiency of historic masonry buildings. A case study: A minor centre in the Abruzzo region, Italy. *Energy Build.* **2014**, *80*, 415–423. [CrossRef]
68. Williamson, J.B.; Stinson, J.; Garnier, C.; Currie, J. In-Situ Monitoring of Thermal Refurbishment on Pre-1919 Properties in Scotland. *Int. J. Sustain. Constr.* **2014**, *2*, 26–33.
69. Sassine, E.; Younsi, Z.; Cherif, Y.; Chauchois, A.; Antczak, E. Experimental determination of thermal properties of brick wall for existing construction in the north of France. *J. Build. Eng.* **2017**, *14*, 15–23. [CrossRef]
70. Sassine, E.; Younsi, Z.; Cherif, Y.; Antczak, E. Thermal performance evaluation of a massive brick wall under real weather conditions via the Conduction Transfer function method. *Case Stud. Constr. Mater.* **2017**, *7*, 56–65. [CrossRef]
71. Evangelisti, L.; Guattari, C.; Gori, P.; Asdrubali, F. Assessment of equivalent thermal properties of multilayer building walls coupling simulations and experimental measurements. *Build. Environ.* **2018**, *127*, 77–85. [CrossRef]
72. Berger, J.; Kadoch, B. Estimation of the thermal properties of an historic building wall by combining modal identification method and optimal experiment design. *Build. Environ.* **2020**, *185*, 107065. [CrossRef]
73. Sassine, E.; Cherif, Y.; Antczak, E. Parametric identification of thermophysical properties in masonry walls of buildings. *J. Build. Eng.* **2019**, *25*, 100801. [CrossRef]
74. Hatır, M.E.; İnce, İ.; Bozkurt, F. Investigation of the effect of microclimatic environment in historical buildings via infrared thermography. *J. Build. Eng.* **2022**, *57*, 104916. [CrossRef]
75. Cruz, C.; Gaju, M.; Gallego, A.; Rescalvo, F.; Suarez, E. Non-Destructive Multi-Feature Analysis of a Historic Wooden Floor. *Buildings* **2022**, *12*, 2193. [CrossRef]
76. Martorana, R.; Capizzi, P. Joint Investigation with Ground Penetrating Radar and Infrared Thermography as a Diagnostic Support for the Restoration of Two Wall Mosaics in the Church of St. Mary of the Admiral in Palermo, Italy. *Heritage* **2022**, *5*, 2298–2314. [CrossRef]
77. Coli, M.; Ciuffreda, A.L.; Marchetti, E.; Morandi, D.; Luceretti, G.; Lippi, Z. 3D HBIM Model and Full Contactless GPR Tomography: An Experimental Application on the Historic Walls That Support Giotto's Mural Paintings, Santa Croce Basilica, Florence—Italy. *Heritage* **2022**, *5*, 2534–2546. [CrossRef]
78. Providakis, C.P.; Mousteraki, M.G.; Providaki, G.C. Operational Modal Analysis of Historical Buildings and Finite Element Model Updating Using α Laser Scanning Vibrometer. *Infrastructures* **2023**, *8*, 37. [CrossRef]
79. Piroddi, L.; Rassu, M. Application of GPR Prospection to Unveil Historical Stratification inside Monumental Buildings: The Case of San Leonardo de Siete Fuentes in Santu Lussurgiu, Sardinia, Italy. *Land* **2023**, *12*, 590. [CrossRef]
80. Santini, S.; Borghese, V.; Baggio, C. HBIM-Based Decision-Making Approach for Sustainable Diagnosis and Conservation of Historical Timber Structures. *Sustainability* **2023**, *15*, 3. [CrossRef]
81. Santini, S.; Cogotti, M.; Baggio, C.; Sabbatini, V.; Sebastiani, C. Field testing for structural behavior of a stratified monumental complex over time: Palazzo Colonna-Barberini and Templum Fortunae Praeneste. *Case Stud. Constr. Mater.* **2023**, *18*, e02152. [CrossRef]
82. de Santoli, L. Guidelines on energy efficiency of cultural heritage. *Energy Build.* **2015**, *86*, 534–540. [CrossRef]
83. Delegou, E.T.; Mourgi, G.; Tsilimantou, E.; Ioannidis, C.; Moropoulou, A. A Multidisciplinary Approach for Historic Buildings Diagnosis: The Case Study of the Kaisariani Monastery. *Heritage* **2019**, *2*, 1211–1232. [CrossRef]
84. Bruno, S.; De Fino, M.; Fatiguso, F. Historic Building Information Modelling: Performance assessment for diagnosis-aided information modelling and management. *Autom. Constr.* **2018**, *86*, 256–276. [CrossRef]
85. Calcerano, F.; Thravalou, S.; Martinelli, L.; Alexandrou, K.; Artopoulos, G.; Gigliarelli, E. Energy and environmental improvement of built heritage: HBIM simulation-based approach applied to nine Mediterranean case-studies. *Build. Res. Inf.* **2023**, 1–23. [CrossRef]
86. Gigliarelli, E.; Calcerano, F.; D'Uffizi, F.; Di Biccari, C.; Mangialardi, G.; Campari, M. From Heritage BIM to BPS, a computational design-based interoperability approach. In Proceedings of the 16th IBPSA Conference, Rome, Italy, 2–4 September 2019.
87. *ISO 19650:2018*; Organization and Digitization of Information about Buildings and Civil Engineering Works, Including Building Information Modelling (BIM)—Information Management Using Building Information Modelling. ISO: Geneva, Switzerland, 2018.

88. National BIM Standard Building. SMART alliance. Part 1: Overview, Principles, and methodologies. In *National Building Information Modeling Standard*; Harris, D., Ed.; National Institute of Building Sciences: Washington, DC, USA, 2007.
89. Eastman, C.M.; Teicholz, P.M.; Sacks, R.; Lee, G. *BIM Handbook: A Guide to Building Information Modeling for Owners, Managers, Designers, Engineers and Contractors*, 3rd ed.; Wiley: Hoboken, NJ, USA, 2018.
90. Pocobelli, D.P.; Boehm, J.; Bryan, P.; Still, J.; Grau-Bové, J. BIM for heritage science: A review. *Herit. Sci.* **2018**, *6*, 30. [CrossRef]
91. Bruno, N.; Roncella, R. HBIM for Conservation: A New Proposal for Information Modeling. *Remote Sens.* **2019**, *11*, 1751. [CrossRef]
92. Mora, R.; Sánchez-Aparicio, L.J.; Maté-González, M.Á.; García-Álvarez, J.; Sánchez-Aparicio, M.; González-Aguilera, D. An historical building information modelling approach for the preventive conservation of historical constructions: Application to the Historical Library of Salamanca. *Autom. Constr.* **2021**, *121*, 103449. [CrossRef]
93. Jouan, P.; Hallot, P. Digital Twin: Research Framework to Support Preventive Conservation Policies. *ISPRS Int. J. Geo-Inf.* **2020**, *9*, 228. [CrossRef]
94. Di Giuda, G.M.; Giana, P.E.; Schievano, M.; Paleari, F. Guidelines to Integrate BIM for Asset and Facility Management of a Public University. In *Digital Transformation of the Design, Construction and Management Processes of the Built Environment*; Springer: Berlin/Heidelberg, Germany, 2020; pp. 309–318. [CrossRef]
95. Bastem, S.S.; Cekmis, A. Development of historic building information modelling: A systematic literature review. *Build. Res. Inf.* **2022**, *50*, 527–558. [CrossRef]
96. Moyano, J.; Carreño, E.; Nieto-Julián, J.E.; Gil-Arizón, I.; Bruno, S. Systematic approach to generate Historical Building Information Modelling (HBIM) in architectural restoration project. *Autom. Constr.* **2022**, *143*, 104551. [CrossRef]
97. Cursi, S.; Martinelli, L.; Paraciani, N.; Calcerano, F.; Gigliarelli, E. Linking external knowledge to heritage BIM. *Autom. Constr.* **2022**, *141*, 104444. [CrossRef]
98. Chiabrando, F.; Donato, V.; Turco, M.L.; Santagati, C. Cultural Heritage Documentation, Analysis and Management Using Building Information Modelling: State of the Art and Perspectives. In *Mechatronics for Cultural Heritage and Civil Engineering*; Springer: Berlin/Heidelberg, Germany, 2018; pp. 181–202. [CrossRef]
99. Bruno, S.; Musicco, A.; Fatiguso, F.; Dell'Osso, G.R. The Role of 4D Historic Building Information Modelling and Management in the Analysis of Constructive Evolution and Decay Condition within the Refurbishment Process. *Int. J. Archit. Herit.* **2021**, *15*, 1250–1266. [CrossRef]
100. Angulo-Fornos, R.; Castellano-Román, M. HBIM as Support of Preventive Conservation Actions in Heritage Architecture. Experience of the Renaissance Quadrant Façade of the Cathedral of Seville. *Appl. Sci.* **2020**, *10*, 2428. [CrossRef]
101. Santagati, C.; Papacharalambous, D.; Sanfilippo, G.; Bakirtzis, N.; Laurini, C.; Hermon, S. HBIM approach for the knowledge and documentation of the St. John the Theologian cathedral in Nicosia (Cyprus). *J. Archaeol. Sci. Rep.* **2021**, *36*, 102804. [CrossRef]
102. Mammoli, R.; Mariotti, C.; Quattrini, R. Modeling the Fourth Dimension of Architectural Heritage: Enabling Processes for a Sustainable Conservation. *Sustainability* **2021**, *13*, 5173. [CrossRef]
103. Simeone, D.; Cursi, S.; Acierno, M. BIM semantic-enrichment for built heritage representation. *Autom. Constr.* **2019**, *97*, 122–137. [CrossRef]
104. Quattrini, R.; Pierdicca, R.; Morbidoni, C. Knowledge-based data enrichment for HBIM: Exploring high-quality models using the semantic-web. *J. Cult. Herit.* **2017**, *28*, 129–139. [CrossRef]
105. Barontini, A.; Alarcon, C.; Sousa, H.S.; Oliveira, D.V.; Masciotta, M.G.; Azenha, M. Development and Demonstration of an HBIM Framework for the Preventive Conservation of Cultural Heritage. *Int. J. Archit. Herit.* **2022**, *16*, 1451–1473. [CrossRef]
106. Vieira, M.; Ribeiro, G.; Alves, K.; Barbosa, J.E.; Isidoro, H.; Martins, T.; Magalhães, B.K.; Almeida, F.E.; Moreira, E.; Mesquita, E. Updating the documentation of a historic building: A case study of the José de Alencar theatre. *J. Build. Pathol. Rehabil.* **2023**, *8*, 36. [CrossRef]
107. Antonopoulou, S.; Bryan, P. *BIM for Heritage: Developing a Historic Building Information Model*; Historic England: Swindon, UK, 2017.
108. Palomar, I.J.; Valldecabres, J.L.G.; Tzortzopoulos, P.; Pellicer, E. An online platform to unify and synchronise heritage architecture information. *Autom. Constr.* **2020**, *110*, 103008. [CrossRef]
109. Spiridigliozzi, G.; Pompei, L.; Cornaro, C.; Santoli, L.D.; Bisegna, F. BIM-BEM support tools for early stages of zero-energy building design. *IOP Conf. Ser. Mater. Sci. Eng.* **2019**, *609*, 072075. [CrossRef]
110. Spiridigliozzi, G.; De Santoli, L.; Cornaro, C.; Basso, G.L.; Barati, S. BIM tools interoperability for designing energy-efficient buildings. *AIP Conf. Proc.* **2019**, *2191*, 020140. [CrossRef]
111. Pompei, L.; Spiridigliozzi, G.; de Santoli, L.; Cornaro, C.; Bisegna, F. Testing the BIM-ladybug tools interoperability: A daylighting simulation workflow. *Build. Simul. Appl.* **2020**, 149–156. Available online: https://www.scopus.com/inward/record.uri?eid=2-s2.0-85090829291&partnerID=40&md5=88ed552c80c27ef0276f99235a5f1984 (accessed on 9 September 2022).
112. Gigliarelli, E.; Calcerano, F.; Calvano, M.; Ruperto, F.; Sacco, M.; Cessari, L. Integrated numerical analysis and Building Information Modeling for Cultural Heritage. In Proceedings of the Conference: Building Simulation Application 2017, Bolzano, Italy, 8–11 February 2017.
113. Nieto-Julián, J.E.; Lara, L.; Moyano, J. Implementation of a TeamWork-HBIM for the Management and Sustainability of Architectural Heritage. *Sustainability* **2021**, *13*, 2161. [CrossRef]

114. Piselli, C.; Romanelli, J.; Di Grazia, M.; Gavagni, A.; Moretti, E.; Nicolini, A.; Cotana, F.; Strangis, F.; Witte, H.J.L.; Pisello, A.L. An Integrated HBIM Simulation Approach for Energy Retrofit of Historical Buildings Implemented in a Case Study of a Medieval Fortress in Italy. *Energies* **2020**, *13*, 2601. [CrossRef]
115. Khodeir, L.M.; Aly, D.; Tarek, S. Integrating HBIM (Heritage Building Information Modeling) Tools in the Application of Sustainable Retrofitting of Heritage Buildings in Egypt. *Procedia Environ. Sci.* **2016**, *34*, 258–270. [CrossRef]
116. Al-Sakkaf, A.; Bagchi, A.; Zayed, T.; Mahmoud, S. Sustainability assessment model for heritage buildings. *Smart Sustain. Built Environ.* **2023**, *12*, 105–127. [CrossRef]
117. Gigliarelli, E.; Calcerano, F.; Martinelli, L.; Cessari, L. A Methodology for Built Heritage Energy and Environmental Improvement: The BEEP Project. In Proceedings of the Heritage for the Future, Science for Heritage, Paris, France, 15–16 March 2022.
118. Croci, G. General methodology for the structural restoration of historic buildings: The cases of the Tower of Pisa and the Basilica of Assisi. *J. Cult. Herit.* **2000**, *1*, 7–18. [CrossRef]
119. Aurigemma, M.G. *Palazzo Firenze in Campo Marzio*; Istituto Poligrafico e Zecca dello Stato, Libreria dello Stato: Foggia, Italy, 2007.
120. Aurigemma, M.G. *Introduzione a Palazzo Firenze*; Società Dante Alighieri, Edilazio: Rome, Italy, 2012.
121. Giovannetti, F. *Manuale del Recupero del Comune di Roma*; DEI: Rome, Italy, 2004.
122. Formenti, C.; Cortelletti, A. *La Pratica del Fabbricare*; Hoepli: Milan, Italy, 1933.
123. Holman, J.P. *Heat Transfer: Tenth Edition*; McGraw-Hill Education: New York, NY, USA, 2010.
124. Vollmer, M. Infrared Thermal Imaging. In *Computer Vision*; Ikeuchi, K., Ed.; Springer International Publishing: Cham, The Switzerland, 2021; pp. 666–670. [CrossRef]
125. Tubi, N.; Silva, M.P.; Ditri, F. *Gli Edifici in Pietra—Recupero e Costruzione—Murature, Solai—Analisi Bioclimatica e Ambientale*; Sistemi Editoriali: Napoli Italy, 2009.
126. Corrado, V.; Ballarini, I.; Corgnati, S.P. *Typology Approach for Building Stock Energy Assessment*; TABULA Project Team: Torino, Italy, 2012.
127. *UNI/TR 11552:2014*; Abaco Delle Strutture Costituenti L'involucro Opaco Degli Edifici—Parametri Termofisici. 2014. Available online: https://store.uni.com/uni-tr-11552-2014 (accessed on 9 September 2022).
128. *UNI 10351:2021*; Materiali da Costruzione—Proprietà Termoigrometriche—Procedura per La Scelta Dei Valori Di Progetto. 2021. Available online: https://store.uni.com/uni-10351-2021 (accessed on 9 September 2022).
129. *UNI EN ISO 6946:2018*; Componenti ed Elementi per Edilizia—Resistenza Termica e Trasmittanza Termica—Metodi di Calcolo. 2018. Available online: https://store.uni.com/uni-en-iso-6946-2018 (accessed on 9 September 2022).
130. D.P.R. 74, Decreto del Presidente della Repubblica 16 aprile 2013, n. 74. Regolamento Recante Definizione dei Criteri Generali in Materia di Esercizio, Conduzione, Controllo, Manutenzione e Ispezione Degli Impianti Termici per la Climatizzazione Invernale ed Estiva degli Edifici e per la preparazione dell'Acqua Calda per usi Igienici Sanitari, a Norma dell'Articolo 4, Comma 1, Lettere a) e c), del d.lgs. 19 Agosto 2005, n. 192 (G.U. n. 149 del 27 Giugno 2013). 2013. Available online: https://www.gazzettaufficiale.it/eli/id/20136/27/13G00114/sg (accessed on 9 September 2022).
131. Gigliarelli, E.; Calcerano, F.; Martinelli, L.; Artopoulos, G.; Thravalou, S.; Alexandrou, K. *Methodology for the Energy Renovation of Heritage Buildings Using BIM.*; CNR Edizioni: Rome, Italy, 2022.